

The influence of equilibrium and nonequilibrium environments on the macroscopic realism through Leggett-Garg inequality

Kun Zhang,¹ Wei Wu,² and Jin Wang^{1,3,*}

¹*Department of Chemistry, State University of New York at Stony Brook, Stony Brook, New York 11794, USA*

²*State Key Laboratory of Electroanalytical Chemistry, Changchun Institute of Applied Chemistry, Chinese Academy of Sciences, Changchun 130022, China*

³*Department of Physics and Astronomy, State University of New York at Stony Brook, Stony Brook, New York 11794, USA*

(Dated: April 10, 2022)

We study macroscopic realism through the Leggett-Garg inequalities (LGI) in two interacting qubit system. The two qubits are coupled either with two Bosonic (thermal and photonic) baths or Fermionic (electronic) baths. We study both how the equilibrium and nonequilibrium environments influence the LGI. One way to characterize the nonequilibrium condition is by the different temperatures (for the Bosonic baths) or the different chemical potentials (for the Fermionic baths). We also study the heat or particle current and the entropy production rate generated by the nonequilibrium environments. Analytical forms of the LGI and the maximal values of LGI based on the quantum master equation beyond secular approximation are derived. The LGI function and its maximal value have separated contributions, the part describing the coherent evolution and the part describing the coupling between the system and environments. The environment coupling part can be from equilibrium environment or nonequilibrium environment. The nonequilibrium dynamics is quantified by the Bloch-Redfield equation which is beyond Lindblad form. We found that the nonequilibriumness quantified by the temperature difference or chemical potential difference can lead to the LGI violation or the increase of the maximal value of LGI, restoring the quantum nature from certain equilibrium cases where LGI is preserved which gives rise to classical realism. The corresponding nonequilibrium thermodynamic cost is quantified by the nonzero entropy production rate. The LGI violation enhancement increases with the increase of the entropy production rate under certain nonequilibrium conditions. Therefore, the LGI violation enhancement can be realized by the thermodynamic nonequilibrium cost. Our results shed on light on the nature of the macroscopic realism and the relationship between the nonequilibriumness and quantum temporal correlation. Our finding of nonequilibrium promoted LGI violation suggests a new strategy for the design of quantum information processing and quantum computational devices to maintain the quantum nature and quantum correlations for long.

I. INTRODUCTION

Quantum correlations, which distinguish the quantum world from classical world, not only are rooted in the fundamental nature of quantum mechanics, but also become valuable resource for quantum information processing [1]. The spacial quantum correlations, known as entanglement [2] or discord [3], show perhaps the most spooky phenomenon in nature. The well-known Bell inequalities [4] was proposed in 1964 to distinguish the classical correlations with the quantum one, and the violation is inconsistent with local hidden variable theory. The nonlocal quantum entanglement (Bell nonlocality or violation of Bell inequalities) has been demonstrated in many experiments since 1972 [5–7].

The temporal quantum correlations, generated by sequential non-commuting measurements on a single system at different times, is different from the classical probabilistic descriptions. Such discrepancy (between classical and quantum) on temporal correlations can be distinguished by the correlation inequalities called Leggett-Garg inequalities (LGI) [8, 9]. LGI is a temporal analogue version of Bell inequalities. Bell inequalities and LGI has the same spirit: the joint probability distribution can not be assigned to all possible measurement results, regardless if the measurements are on separated space or time [10]. LGI was firstly motivated to demonstrate

macroscopic coherence, namely how to justify the existence of macroscopic superposition state. LGI and its many variants can test the realism of physical state: before the measurements, the system is in definite states with distinct observable values, which is also the essence of hidden variable theory. Violation of LGI implies that the system is undergoing the quantum mechanical time evolution which is beyond classical probability description. Although Bell inequalities and LGI share the same spirit, LGI is not sufficient and necessary condition for testing macroscopic realism [11]. For example, the Wigner’s form of LGI can be violated while the original LGI are preserved (for non-ideal measurements) [12]. The sufficient and necessary condition for macroscopic realism was proposed called no-signaling in time condition [13]. Such condition is characterized by equalities instead of inequalities in LGI. Experimental studies may still favor LGI, since inequalities are more easily tested. The quantum experiments based on different platforms demonstrated the violation of LGI and its variants, see [14–20].

Quantum coherence is notoriously fragile due to the coupling with the environments. This leads to decoherence [21–23]. Decoherence has to be included when studying violations of LGI in real world. When the system is coupled with the environments (also called reservoirs or baths in this paper), the dynamics between the system and the environments can be classified as Markovian (memoryless) [22, 24] or non-Markovian (with memory effect) [25]. Both Markovian [26–31] and non-Markovian [32, 33] effects on violations of LGI

* Email: jin.wang.1@stonybrook.edu

have been studied before. However, the non-Markovian case requires special care since quantum coherent evolution can be rewritten as a non-Markovian rate equation which can violate LGI [9, 34].

The effects of the environments to the system can be classified as equilibrium and nonequilibrium, where the nonequilibrium condition is quantified as the temperature difference or the chemical potential difference of the environments or baths. The nonequilibrium condition represents the degree of the energy or matter exchange between the system and the reservoirs respectively. Coherence [35–37] or entanglement [38–46] generated and controlled from (the one and therefore equilibrium) environment have been intensely studied in last twenty years, due to their potential applications in quantum information processing. Nonequilibrium environments [47] draw more attentions in recent years. Nonequilibrium environments have their own significance for maintaining and enhancing long time coherence [48–50] or entanglement [51–62]. At equilibrium scenario, coupling with the environment has only negative influence on violation of LGI [27–29]. However, the steady state coherence generated under nonequilibrium condition [48–50] seems to suggest that nonequilibriumness may contribute to or enhance the violation of LGI. Only very limited numbers of studies have been devoted to the issue of how the nonequilibriumness (energy or particle exchange with the system) influences quantum dynamical nature of the system [31, 63].

To address the question how equilibrium and nonequilibrium environments influences LGI, we study the following setup: two coupled qubit system (with different frequencies) immersed into two individual reservoirs respectively. The two reservoirs can have the same or different temperatures (Bosonic baths) or chemical potentials (Fermionic baths). Weak coupling between the system and the environments and Markovian dynamics are assumed in the model. The dynamics of the system is described by Bloch-Redfield equation [64, 65], without the secular approximation made in the Lindblad equation. The Lindblad equation is not used here because the nonequilibrium steady state coherence is neglected by the secular approximation in the Lindblad equation [37, 48–50, 59]. Specifically, if the secular approximation has been applied, population space and coherent space will be decoupled. Moreover, LGI is dependent on local observables (local measurement performed on one qubit). Furthermore, if the secular approximation is applied, LGI will have symmetric response to temperature difference even under nonequilibrium environments [31]. However, the Bloch-Redfield equation is criticized by non-positivity of density matrix evolution in certain parameter regimes. The positivity of Bloch-Redfield equation may be recovered by the initial conditions [66] or further approximations [67, 68]. The validity of Bloch-Redfield equation is beyond scope of the study in this paper. Instead, we circumvent the positivity issue by concentrating on the parameter regimes which give positive density matrix.

In our study, we consider the equilibrium and nonequilibrium steady state as initial state for LGI. Therefore, only the time interval of sequential measurement matters. We give analytical results about steady state at both equilibrium and

nonequilibrium scenarios. In nonequilibrium case, the two reservoirs are sustained with constant temperature difference or chemical potential difference if the two baths are Bosonic or Fermionic respectively. Sequentially measuring one local qubit gives temporal correlations of the local observable. We analytically find the LGI based on the weak coupling assumption (we approximate LGI up to first order coupling strength between the system and the environments). The zero-th order (in terms of coupling strength) can be viewed as coherent evolution part and the first order part describes the effects on LGI from the dynamical coupling between the system and the environments. The maximal value of LGI (MLGI) can be viewed as the degree of LGI violations.

In equilibrium case, MLGI has non-monotonic relation with common temperature or chemical potential. In the low temperature regime, increasing the temperature can increase the population of the excited states, which are nonlocal. In the high temperature regime, increasing the temperature leads to stronger thermal effects (decoherence). In nonequilibrium scenario, MLGI can be enhanced by the nonequilibrium conditions: the temperature difference or the entropy production rate in Bosonic environments; the chemical potential difference or the entropy production rate in Fermionic environments. The LGI violation enhancement has a thermodynamic cost quantified by the nonzero entropy production rate. The Bosonic enhancement is only realized at low mean temperature regime. If we choose to measure the qubit 1, then MLGI has greater enhancement if the qubit 1 is coupled with lower temperature. Note that the Lindblad will give symmetric result: the qubit 1 coupled with lower temperature T_1 and the qubit 2 coupled with higher temperature T_2 give the same MLGI when qubit 1 is coupled with higher temperature T_2 and qubit 2 is coupled with lower temperature T_1 . In other words, Lindblad does not characterize well the nonequilibrium dynamics. We obtained MLGI enhancement from chemical potential difference (Fermionic baths) when the mean chemical potential is away from the resonant point. The resonance occurs when the mean chemical potential equals to the mean energy of the two-qubit system. We have also studied the LGI violation when the two-qubit system has detuned energy splitting. We got larger MLGI (than the equilibrium case) when the low frequency qubit is coupled with the high temperature bath or high chemical potential bath and high frequency qubit is coupled with the low temperature bath or high chemical potential.

Rest of the paper is organized as follow. Sec. II reviews time correlation functions and LGI. Sec. III presents the dynamic quantum master equation of the system and the analytical form of the steady state. We study LGI and MLGI at equilibrium and nonequilibrium cases in Sec. IV and Sec. V respectively. The results are based on analytical expressions and are demonstrated numerically. The last section gives the conclusion. The detailed expressions for the Bloch-Redfield equation and the heat or particle current are presented in the Appendix.

II. LEGGET-GARG INEQUALITIES

In classical probabilistic theory, the results of measurements performed at different times t_j and t_l can be described by the joint probability $P(Q_j, t_j; Q_l, t_l)$. Here Q_j is the measurement value at t_j . The correlation function characterizing the measurement results at t_j and t_l is defined as

$$C_{\text{cl}}(t_j, t_l) = \sum_{Q_j, Q_l} Q_j Q_l P(Q_j, t_j; Q_l, t_l) \quad (1)$$

Subscript cl distinguishes the correlation functions from quantum case.

Macroscopic realism is based on *Macrorealism per se* and *Non-invasive measurability* assumptions [8, 9]. *Macrorealism per se* means that the physical object is in one of the distinct states (with different observable values) irrespect to the measurements. *Non-invasive measurability* means measurements (in principle) can reveal object's state without influencing the object itself. *Non-invasive measurability* also implies that the two-time measurement results can always be obtained from the marginal of a three-time probability distribution. Combined with the completeness relation of the three-time probability distribution, the correlation functions satisfy the inequality

$$C_{\text{cl}}(t_1, t_2) + C_{\text{cl}}(t_2, t_3) - C_{\text{cl}}(t_1, t_3) \leq 1 \quad (2)$$

which is called LGI [9].

In quantum mechanics, there is no unique analogue of classical correlation function defined in (1), because of the operator ordering. Suppose we have dichotomic observables $Q_j = \pm 1$. We can define the correlation functions by taking the real part of the observables:

$$C_{\text{q}}(t_j, t_l) = \frac{1}{2} \text{Tr} (\{Q(t_j), Q(t_l)\} \rho) = \text{Re} \text{Tr} (Q(t_j)Q(t_l)\rho) \quad (3)$$

The subscript q means quantum. It can be interpreted exactly the same as the classical correlation function: the correlation between the two measurement results at time t_j and t_l . Such interpretation is only valid for dichotomic observables (with values ± 1). Note that the imaginary part of $\text{Tr}(Q(t_j)Q(t_l)\rho)$ is a measure of non-commutativity for observables $Q(t_j)$ and $Q(t_l)$ (without classical analog).

In the standard description of quantum mechanics, *Macrorealism per se* assumption is violated because of the superposition principle. *Non-invasive measurability* is not valid due to the measurement wavefunction collapse in quantum mechanics. Note that LGI can be generalized into multi-time measurement. The detailed review about LGI can be found in [9]. In practice, we can keep the two-time intervals in the three-time measurements to be the same, i.e., $t_2 - t_1 = t_3 - t_2 = t$. For the steady state density matrix, the initial time t_1 is trivial. We define the function

$$\mathcal{I}(t, \rho^{\text{ss}}) = 2 \text{Re} (\langle Q(t)Q \rangle - \langle Q(2t)Q \rangle) \quad (4)$$

with $Q = Q(t = 0)$. Function $\mathcal{I}(t, \rho^{\text{ss}})$ (as function of time interval t and steady state ρ^{ss}) is the quantum expression of

LGI defined in (2), combined with the equal time interval (the time of three measurements) and the steady state condition. We define the maximal value of $\mathcal{I}(t, \rho^{\text{ss}})$ by

$$\mathcal{I}_{\text{max}}(\rho^{\text{ss}}) = \max_{t \geq 0} \{\mathcal{I}(t, \rho^{\text{ss}})\} - 1 \quad (5)$$

The minimal value of $\mathcal{I}_{\text{max}}(\rho^{\text{ss}})$ is 0 since we have

$$\mathcal{I}(0, \rho^{\text{ss}}) = 1 \quad (6)$$

Violation of LGI in (2) gives $\mathcal{I}_{\text{max}}(\rho^{\text{ss}}) > 0$, which suggests that the quantum evolution (of system) is beyond the classical descriptions (no joint probability distribution for observables at different times) [9]. Unitary evolution (full quantum description) of quantum state (pure steady state) gives the maximal value of $\mathcal{I}_{\text{max}}(\rho^{\text{ss}})$. For two-level (qubit) system, the maximal value of $\mathcal{I}_{\text{max}}(\rho^{\text{ss}})$ is 1/2. We have the range:

$$0 \leq \mathcal{I}_{\text{max}}(\rho^{\text{ss}}) \leq \frac{1}{2} \quad (7)$$

In the experiments, MLGI is a natural quantity characterizing the degree of quantumness on the evolution of the system.

III. QUANTUM EVOLUTION OF MASTER EQUATION AND STEADY STATE

A. Model

We study a two coupled two-level (qubit) system (with different transition frequencies) individually coupled to two Bosonic or Fermionic baths respectively with different temperatures or chemical potentials. The free Hamiltonian of the system (coupled two qubits) and the environments are given by

$$H_S = \omega_1 |e_1\rangle\langle e_1| + \omega_2 |e_2\rangle\langle e_2| + \frac{\lambda}{2} (\sigma_1^+ \sigma_2^- + \sigma_1^- \sigma_2^+), \quad (8)$$

$$H_R = \sum_k \omega_{bk} b_k^\dagger b_k + \sum_k \omega_{ck} c_k^\dagger c_k \quad (9)$$

where ω_1 and ω_2 represent the energy splittings (transition frequencies) for the first and second qubit respectively; state $|e_1\rangle$ or $|e_2\rangle$ is the excitation in the first or second qubit; the ground state has energy 0; the third term in H_S describes the coupling between the two qubits and λ is the coupling strength between qubit 1 and qubit 2; operators $\sigma_1^+ = |e_1\rangle\langle g_1|$ and $\sigma_2^+ = |e_2\rangle\langle g_2|$ are the raising (creation) operators for the qubit one and the qubit two respectively; Bosonic bath gives the commutative relation $[b_k, b_{k'}^\dagger] = \delta_{kk'}$, $[b_k, b_{k'}] = 0$ and Fermionic bath gives the anti-commutative relation $\{b_k, b_{k'}^\dagger\} = \delta_{kk'}$, $\{b_k, b_{k'}\} = 0$; the two baths have the energy spectral ω_{bk} and ω_{ck} for the k -th mode (b denotes the first bath coupled with qubit number 1 and c denotes the second bath coupled with qubit number 2). The constant $\hbar = 1$ is set to 1 for convenience.

Model having the Hamiltonian H_S in (8) can be understood as two spatial separated atoms coupled through the dipole-dipole interaction [69]. In the language of spin chain, Hamiltonian H_S in (8) describes the Heisenberg XY model ($\sigma_x \sigma_x$

and $\sigma_y\sigma_y$ interaction) and the two spins are subjected to inhomogeneous magnetic field (different transition frequencies) [40, 41, 52, 70]. If the two-level system is understood as (spin-degenerate) quantum dots: $|g\rangle$ as empty site and $|e\rangle$ as occupied site, the coupling between the two qubits is essentially the non-interaction tunneling [51, 62]. Note that the Hamiltonian H_S in (8) does not include the interdot Coulomb interaction of the two sites (as toy model for double quantum dots).

Because of the dipole-dipole interaction, atomic basis is not the eigenstate. The system forms the dimer eigenstates (with the new eigenenergies) defined by:

$$\begin{aligned} \omega_{gg} &= 0, & |1\rangle &= |gg\rangle, \\ \omega'_1 &= \bar{\omega} - \frac{1}{2}\sqrt{\Delta\omega^2 + \lambda^2}, & |2\rangle &= \cos\frac{\theta}{2}|eg\rangle + \sin\frac{\theta}{2}|ge\rangle, \\ \omega'_2 &= \bar{\omega} + \frac{1}{2}\sqrt{\Delta\omega^2 + \lambda^2}, & |3\rangle &= -\sin\frac{\theta}{2}|eg\rangle + \cos\frac{\theta}{2}|ge\rangle, \\ \omega_{ee} &= \omega_1 + \omega_2, & |4\rangle &= |ee\rangle \end{aligned} \quad (10)$$

We use short notations: $|eg\rangle = |e_1\rangle \otimes |g_2\rangle$. Here $\bar{\omega} = (\omega_1 + \omega_2)/2$ is the mean energy splitting and $\Delta\omega = \omega_1 - \omega_2$ is the degree of energy detuning. The dipole-dipole interaction is relatively weak. We limit the coupling strength in the regime $\lambda < \sqrt{\omega_1\omega_2}$. The angle θ is defined by

$$\theta = \begin{cases} \arctan(\lambda/\Delta\omega), & \text{if } \Delta\omega < 0 \\ \arctan(\lambda/\Delta\omega) - \pi, & \text{if } \Delta\omega > 0 \end{cases} \quad (11)$$

The identical two qubits ($\omega_1 = \omega_2 = \omega$) gives $\theta = -\pi/2$. And the eigenstate $|2\rangle$ and $|3\rangle$ are Bell-like states (maximal entangled two-qubit states). The weak-interqubit coupling $\lambda < \sqrt{\omega_1\omega_2}$ gives the ground state $|gg\rangle$. We have quantum phase transition [71] at $\lambda = \sqrt{\omega_1\omega_2}$: state $|2\rangle$ will be ground state if $\lambda = \sqrt{\omega_1\omega_2}$.

We can expand the lowering (annihilation) operators σ_l^- (with $l = 1, 2$) and raising (creation) operators σ_l^+ into the basis of eigenstates $|j\rangle$ (with $j = 1, 2, 3, 4$):

$$\sigma_1^- = \eta_1 + \xi_1, \quad \sigma_2^- = \eta_2 + \xi_2 \quad (12)$$

with the operators η and ξ defined in the energy basis

$$\eta_1 = \cos\frac{\theta}{2}(|1\rangle\langle 2| + |3\rangle\langle 4|), \quad (13a)$$

$$\eta_2 = \cos\frac{\theta}{2}(|1\rangle\langle 2| - |3\rangle\langle 4|), \quad (13b)$$

$$\xi_1 = \sin\frac{\theta}{2}(|2\rangle\langle 4| - |1\rangle\langle 3|), \quad (13c)$$

$$\xi_2 = \sin\frac{\theta}{2}(|2\rangle\langle 4| + |1\rangle\langle 3|) \quad (13d)$$

Similarly, the raising operators σ_l^+ can be reformulated with the operators η_l^\dagger and ξ_l^\dagger (with $l = 1, 2$).

We adopt the rotation wave approximation (neglecting oscillations with high frequency) to describe the interaction between the system and the environments:

$$H_{SR} = \sum_k g_k (\sigma_1^- b_k^\dagger + \sigma_1^+ b_k) + \sum_k h_k (\sigma_2^- c_k^\dagger + \sigma_2^+ c_k) \quad (14)$$

where g_k and h_k are the coupling strengths between the system and the environments. We can assume that g_k and h_k are both real numbers without losing generality. When we have the Bosonic environments (operators b_k and c_k follow the commutative relation), our model describes two-atomic system or two-spin system interacting with photonic or thermal baths. When we have Fermionic environments (operators b_k and c_k follow the anti-commutative relation), our model describes double quantum dots coupled with two metal leads.

In the interaction picture, the Hamiltonian H_{SR} (14) takes the form

$$\begin{aligned} H_{SR}(t) &= \sum_k g_k (\eta_1 e^{-i\omega'_1 t} + \xi_1 e^{-i\omega'_2 t}) b_k^\dagger e^{i\omega_{bk} t} + \text{h.c.} \\ &+ \sum_k h_k (\eta_2 e^{-i\omega'_1 t} + \xi_2 e^{-i\omega'_2 t}) c_k^\dagger e^{i\omega_{ck} t} + \text{h.c.} \end{aligned} \quad (15)$$

where h.c. is short for Hermitian conjugate. The physical meaning of operators η_l and ξ_l (13a)-(13d) are clear: operators η_l are lowering the energy ω'_1 and operators ξ_l are lowering the energy ω'_2 .

B. Quantum Master Equation

Based on the weak-coupling (between system and environment) and Born-Markov approximations, the dynamics of system (in the interaction picture) is governed by the quantum master equation for reduced density matrix (after tracing over the baths): [22]

$$\frac{d\rho_I(t)}{dt} = -\int_0^\infty ds \text{Tr}_R [H_{SR}(t), [H_{SR}(t-s), \rho_I(t) \otimes \rho_R]] \quad (16)$$

where $\rho_I(t) = \exp(-iH_{ST})\rho_S\exp(iH_{ST})$ and ρ_R is the density matrix of the two baths in their thermal equilibrium states. Here i is the imaginary unit $i = \sqrt{-1}$. The above equation is called Bloch-Redfield equation [22, 64, 65]. For our model described by the interaction Hamiltonian H_{SR} defined in (14), we have the Bloch-Redfield equation (back to Schrödinger's picture):

$$\frac{d\rho_S}{dt} = i[\rho_S, H_S] + \sum_{l=1}^2 \mathcal{D}_l[\rho] \quad (17)$$

with the dissipators expressed as ($l = 1, 2$)

$$\begin{aligned} \mathcal{D}_l[\rho] &= \alpha_l(\omega'_1) (\eta_l^\dagger \rho \eta_l + \eta_l^\dagger \rho \xi_l - \eta_l \eta_l^\dagger \rho - \xi_l \eta_l^\dagger \rho + \text{h.c.}) \\ &+ \alpha_l(\omega'_2) (\xi_l^\dagger \rho \xi_l + \eta_l^\dagger \rho \xi_l - \xi_l \xi_l^\dagger \rho - \eta_l \xi_l^\dagger \rho + \text{h.c.}) \\ &+ \beta_l(\omega'_1) (\eta_l \rho \eta_l^\dagger + \eta_l \rho \xi_l^\dagger - \eta_l^\dagger \eta_l \rho - \xi_l^\dagger \eta_l \rho + \text{h.c.}) \\ &+ \beta_l(\omega'_2) (\xi_l \rho \xi_l^\dagger + \eta_l \rho \xi_l^\dagger - \xi_l^\dagger \xi_l \rho - \eta_l^\dagger \xi_l \rho + \text{h.c.}) \end{aligned} \quad (18)$$

Here the coefficients are

$$\alpha_l(\omega) = J_l(\omega) n_l(\omega), \quad \beta_l(\omega) = J_l(\omega)(1 \pm n_l(\omega)) \quad (19)$$

with the coupling spectrum of the two baths defined as:

$$J_1(\omega) = \pi \sum_k g_k^2 \delta(\omega - \omega_{bk}), \quad J_2(\omega) = \pi \sum_k h_k^2 \delta(\omega - \omega_{ck}) \quad (20)$$

Here the plus sign in $\beta_l(\omega)$ is for Bosonic bath and the minus sign is for Fermionic bath. Variable $n_l(\omega)$ is the mean occupation number of particles with the energy ω at temperature T_l and chemical potential μ_l for the l -th bath, namely

$$n_l(\omega) = \frac{1}{\exp((\omega - \mu_l)/T_l) \mp 1} \quad (21)$$

The minus sign is for Bosonic bath (Bose-Einstein distribution) and plus sign is for Fermionic bath (Fermi-Dirac distribution). Boltzmann constant is set to be 1. Photons or phonons have negligible self-interactions. We set $\mu_1 = \mu_2 = 0$ both for equilibrium ($T_1 = T_2 = T$) and nonequilibrium ($T_1 \neq T_2$) Bosonic baths. And we consider the temperature equilibrium ($T_1 = T_2 = T$) for Fermionic baths both for equilibrium chemical potential ($\mu_1 = \mu_2 = \mu$) and nonequilibrium chemical potential ($\mu_1 \neq \mu_2$) cases, especially in low temperature regime.

Operators η_l defined in (13a)-(13b) and ξ_l defined in (13c)-(13d) characterize the transitions with different frequencies (η_l is for ω'_1 and ξ_l is for ω'_2). In the interaction picture, cross terms in the dissipators in (18), such as $\eta_l^\dagger \rho \xi_l$, are usually considered as oscillating processes and therefore often neglected under fast oscillations (secular approximation). After secular approximation, Bloch-Redfield equation becomes the Lindblad form. Since the cross terms couple the population and coherent space of the density matrix, dropping the crossing terms gives zero steady state coherence (in eigenstate representation), see [49, 50, 59]. Coherence is crucial for the violation of LGI. Therefore, *we keep the cross terms in our study and apply the master equation without secular approximation, or the Bloch-Redfield equation for time evolution of the system.*

C. Steady State Solutions

The steady state solution of the Bloch-Redfield equation in a similar setting (for the study of a different problem) had been obtained in [59]. Here we follow the similar procedure. We can reformulate the Bloch-Redfield equation with the form (17) in the Liouville space, where the system density matrix takes the vector form

$$|\rho_S\rangle = (\rho_{11}, \rho_{22}, \rho_{33}, \rho_{44}, \rho_{23}, \rho_{32})^T \quad (22)$$

with T as the matrix transpose. Other coherent terms (such as ρ_{14} and ρ_{41}) are decoupled with the population terms and therefore can be dropped in steady state solution. The Bloch-Redfield equation (17) has the matrix form:

$$\frac{d}{dt}|\rho_S\rangle = \mathcal{M}|\rho_S\rangle \quad (23)$$

The expressions of the matrix elements \mathcal{M} are given in Appendix A.

The reduced system density matrix both can be grouped into two parts: $|\rho_S\rangle = (\rho_p, \rho_c)^T$ with population terms ρ_p (diagonal terms) and coherent terms ρ_c (off-diagonal terms). Under the same arguments, dynamic matrix \mathcal{M} has the block forms:

$$\mathcal{M} = \begin{pmatrix} \mathcal{M}_{pp} & \mathcal{M}_{pc} \\ \mathcal{M}_{cp} & \mathcal{M}_{cc} \end{pmatrix} \quad (24)$$

The steady state is given by

$$\mathcal{M}|\rho_S^{ss}\rangle = 0 \quad (25)$$

The superscript “ss” stands for steady state. The coherent terms can be substituted by

$$\rho_c = -\mathcal{M}_{cc}^{-1} \mathcal{M}_{cp} \rho_p \quad (26)$$

with invertible block matrix \mathcal{M}_{cc} . Then we define the steady state population matrix \mathcal{A} as

$$\mathcal{A} = \mathcal{M}_{pp} - \mathcal{M}_{pc} \mathcal{M}_{cc}^{-1} \mathcal{M}_{cp} \quad (27)$$

which satisfies

$$\mathcal{A}|\rho_p^{ss}\rangle = 0 \quad (28)$$

Note that the overall constant in \mathcal{A} gives the same steady state solution. The matrix elements of the steady state population matrix \mathcal{A} , both for Bosonic and Fermionic bath, are presented in Appendix B.

In the following, we consider the symmetric constant coupling spectrum:

$$J_1(\omega) = J_2(\omega) = J \quad (29)$$

To simplify the steady state expressions ρ_S^{ss} , we introduce the following notations:

$$\tilde{n}_1(\theta, \omega'_1) = \cos^2 \frac{\theta}{2} n_1(\omega'_1) + \sin^2 \frac{\theta}{2} n_2(\omega'_1), \quad (30a)$$

$$\tilde{n}_2(\theta, \omega'_2) = \sin^2 \frac{\theta}{2} n_1(\omega'_2) + \cos^2 \frac{\theta}{2} n_2(\omega'_2), \quad (30b)$$

$$\Delta n_1(\theta, \omega'_1) = \frac{1}{2} \sin \theta (n_2(\omega'_1) - n_1(\omega'_1)), \quad (30c)$$

$$\Delta n_2(\theta, \omega'_2) = \frac{1}{2} \sin \theta (n_2(\omega'_2) - n_1(\omega'_2)) \quad (30d)$$

To avoid tedious notations, we set

$$\tilde{n}_l \equiv \tilde{n}_l(\theta, \omega'_l), \quad \Delta n_l \equiv \Delta n_l(\theta, \omega'_l) \quad (31)$$

with $l = 1, 2$. Here \tilde{n}_l can be viewed as the mean particle occupation number weighted by the mixing angle θ in the two baths with the energy ω'_l . And Δn_l describes difference in occupation number and therefore the degree of the nonequilibriumness which vanish at the equilibrium case $T_1 = T_2$ and $\mu_1 = \mu_2$.

1. Steady state solution for Bosonic bath

Directly solving the steady state equation (28) for Bosonic baths (matrix \mathcal{A}^b for Bosonic baths has the elements in (B2)-(B17)) gives the steady solution [59]:

$$\rho_{11}^b = \frac{1}{\mathcal{N}^b} \left((1 + \tilde{n}_1)(1 + \tilde{n}_2) - \frac{\kappa^b a_1 a_2}{4(1 + \tilde{n}_1 + \tilde{n}_2)} \right), \quad (32a)$$

$$\rho_{22}^b = \frac{1}{\mathcal{N}^b} \left(\tilde{n}_1(1 + \tilde{n}_2) + \frac{\kappa^b a_2 a_3}{4(1 + \tilde{n}_1 + \tilde{n}_2)} \right), \quad (32b)$$

$$\rho_{33}^b = \frac{1}{\mathcal{N}^b} \left(\tilde{n}_2(1 + \tilde{n}_1) + \frac{\kappa^b a_1 a_4}{4(1 + \tilde{n}_1 + \tilde{n}_2)} \right), \quad (32c)$$

$$\rho_{44}^b = \frac{1}{\mathcal{N}^b} \left(\tilde{n}_1 \tilde{n}_2 - \frac{\kappa^b a_3 a_4}{4(1 + \tilde{n}_1 + \tilde{n}_2)} \right) \quad (32d)$$

Here κ^b is defined as

$$\kappa^b = \frac{\tilde{n}_1 + \tilde{n}_2 + 1}{(\tilde{n}_1 + \tilde{n}_2 + 1)^2 + (\Omega/2J)^2} \quad (33)$$

with the transition frequency given as

$$\Omega = \omega'_2 - \omega'_1 = \sqrt{\Delta\omega^2 + \lambda^2} \quad (34)$$

Note that κ^b is also defined in the population matrix \mathcal{A}^b , see (B1). And the other parameters are:

$$a_1 = \Delta n_2 - \Delta n_1(3 + 2\tilde{n}_1 + 2\tilde{n}_2), \quad (35a)$$

$$a_2 = \Delta n_1 - \Delta n_2(3 + 2\tilde{n}_1 + 2\tilde{n}_2), \quad (35b)$$

$$a_3 = \Delta n_2 + \Delta n_1(1 + 2\tilde{n}_1 + 2\tilde{n}_2), \quad (35c)$$

$$a_4 = \Delta n_1 + \Delta n_2(1 + 2\tilde{n}_1 + 2\tilde{n}_2), \quad (35d)$$

The normalization \mathcal{N}^b is

$$\mathcal{N}^b = (1 + 2\tilde{n}_1)(1 + 2\tilde{n}_2) - 4\kappa_b \Delta n_1 \Delta n_2 (1 + \tilde{n}_1 + \tilde{n}_2) \quad (36)$$

The superscript b stands for the Bosonic reservoir setup. We omit the superscript “ss” for steady state.

The steady state coherence is given by (26). We have

$$\rho_{23}^b = \rho_{32}^b * = \frac{1}{\mathcal{N}_b} \left(\frac{\Delta n_1(1 + 2\tilde{n}_2) + \Delta n_2(1 + 2\tilde{n}_1)}{2(1 + \tilde{n}_1 + \tilde{n}_2) - i\Omega/J} \right) \quad (37)$$

which vanishes if $\Delta n_1 = \Delta n_2 = 0$, namely at the equilibrium case, off-diagonal terms of the reduced density matrix at steady state in the energy basis are always zero. The star $*$ represents the complex conjugate.

Parameters a_j with $j = 1, 2, 3, 4$ defined in (35a)-(35d) solely characterize the nonequilibrium effects, since they all vanish at equilibrium cases. We can view the second terms in (32a)-(32d) as the nonequilibrium corrections which are proportional to the square of coupling strength J^2 (since κ^b (33) is proportional to J^2). Although J^2 is negligible (weak coupling assumption), the nonequilibrium correction terms such as $J^2 \Delta \tilde{n}_l^2$ are not bounded (only for Bosonic baths). The first term of the steady state population in (32a)-(32d) can only reveal part of the nonequilibrium effects (the mean properties of

the two baths) if we have intermediate temperature difference. In other words, Lindblad can be used to characterize *some* nonequilibrium results [31, 53, 54]. However, we will see later that LGI and MLGI obtained by Bloch-Redfield equation can have significant deviations from those characterized by Lindblad, due to the dynamic differences.

Equilibrium case ($T_1 = T_2 = T$) gives vanishing Δn_i with $i = 1, 2$ (defined in (30c) and (30d)). Therefore, we do not have coherence ρ_{23}^b in energy basis. We have the equilibrium steady state:

$$\begin{aligned} \rho_{11}^{b,e} &= \frac{1}{\mathcal{N}^{b,e}} (1 + \tilde{n}_1)(1 + \tilde{n}_2), & \rho_{22}^{b,e} &= \frac{1}{\mathcal{N}^{b,e}} \tilde{n}_1(1 + \tilde{n}_2), \\ \rho_{33}^{b,e} &= \frac{1}{\mathcal{N}^{b,e}} \tilde{n}_2(1 + \tilde{n}_1), & \rho_{44}^{b,e} &= \frac{1}{\mathcal{N}^{b,e}} \tilde{n}_1 \tilde{n}_2 \end{aligned} \quad (38)$$

with the normalization

$$\mathcal{N}^{b,e} = (1 + 2\tilde{n}_1)(1 + 2\tilde{n}_2) \quad (39)$$

The superscript e reminds the equilibrium situation. The equilibrium steady state satisfies the canonical ensemble distribution. At low temperatures, the system stays at ground state with high probability:

$$\lim_{T \rightarrow 0} \rho_{11}^{b,e} = 1 \quad (40)$$

At high temperatures, we have the equally mixed state:

$$\lim_{T \rightarrow \infty} \rho_{jj}^{b,e} = \frac{1}{4} \quad (41)$$

with $j = 1, 2, 3, 4$.

2. Steady state solution for Fermionic bath

When the system is coupled with two Fermionic baths (double quantum dots as the system), we have the steady state population matrix \mathcal{A}^f with matrix elements given in (B18)-(B31). We can solve the reduced steady state density matrix [59]:

$$\rho_{11}^f = (1 - \tilde{n}_1)(1 - \tilde{n}_2) - \frac{\kappa^f}{4} (\Delta n_1 + \Delta n_2)^2, \quad (42a)$$

$$\rho_{22}^f = \tilde{n}_1(1 - \tilde{n}_2) + \frac{\kappa^f}{4} (\Delta n_1 + \Delta n_2)^2, \quad (42b)$$

$$\rho_{33}^f = \tilde{n}_2(1 - \tilde{n}_1) + \frac{\kappa^f}{4} (\Delta n_1 + \Delta n_2)^2, \quad (42c)$$

$$\rho_{44}^f = \tilde{n}_1 \tilde{n}_2 - \frac{\kappa^f}{4} (\Delta n_1 + \Delta n_2)^2 \quad (42d)$$

with κ^f defined as

$$\kappa^f = \frac{1}{1 + (\Omega/2J)^2} \quad (43)$$

The superscript f means the Fermionic bath setup. The corresponding coherence terms of the reduced density matrix are

$$\rho_{23}^f = \rho_{32}^f * = \frac{\Delta n_1 + \Delta n_2}{2 - i\Omega/J} \quad (44)$$

which is zero if $\Delta n_1 = \Delta n_2 = 0$. Nonequilibrium corrections (second terms in (42a)-(42d)) is proportional to $J^2 \Delta n_l^2$. Unlike the Bosonic environments, the particle occupation number difference $|\Delta n_l| < 1/2$ is bounded in Fermionic case. Therefore, for $J \ll \Omega$, the Lindblad form can give reasonable description for effects of the nonequilibrium Fermionic environments.

The equilibrium steady state ($T_1 = T_2 = T$ and $\mu_1 = \mu_2 = \mu$) is the special case of (42a)-(42d) with $\Delta n_1 = \Delta n_2 = 0$:

$$\begin{aligned} \rho_{11}^{\text{fe}} &= (1 - \tilde{n}_1)(1 - \tilde{n}_2), & \rho_{22}^{\text{fe}} &= \tilde{n}_1(1 - \tilde{n}_2) \\ \rho_{33}^{\text{fe}} &= \tilde{n}_2(1 - \tilde{n}_1), & \rho_{44}^{\text{fe}} &= \tilde{n}_1\tilde{n}_2 \end{aligned} \quad (45)$$

which satisfies the grand canonical ensemble distribution ($\mu \neq 0$). At low temperature, we reach

$$\lim_{\mu \rightarrow 0} \rho_{11}^{\text{fe}} = 1 \quad (46)$$

The double dots are both empty. When we have high chemical potential (low temperature), we reach

$$\lim_{\mu \rightarrow \infty} \rho_{44}^{\text{fe}} = 1 \quad (47)$$

We have two occupied sites.

IV. LEGGET-GARG INEQUALITY VIOLATION IN EQUILIBRIUM CASE

LGI defined in (2) states the constraints on the probability distributions (simultaneously) for observables at different times. Quantum mechanical description is not equivalent to the classical probabilistic description. The degree of LGI violation is characterized by the maximal value of LGI (MLGI). In this section, we study the LGI function $\mathcal{I}(t, \rho^{\text{ss}})$ (quantum version of LGI) defined in (4) and its maximal value $\mathcal{I}_{\max}(\rho^{\text{ss}})$ defined in (5) when the system is coupled with the equilibrium environments (two Bosonic baths have the same temperatures or two Fermionic baths have both the same temperatures and chemical potentials). The dynamics of the system is described by the Bloch-Redfield equation (17). It is difficult to give the closed expression for the time evolution operator given any time t . In the following, we calculate the time evolution operator in a perturbative way, namely the time evolution operator in the zeroth and the first order of the coupling J defined in (20). Such perturbation is valid if the system and bath are weakly coupled and the equilibrium temperature is relative low. The weakly coupling condition is also the assumption for deriving the Bloch-Redfield equation (17). We will check our analytical expressions with numerical results.

A. Legget-Garg Inequality in the Zeroth Order of Coupling

The time evolution operator for the reduced density matrix (two qubit system) is generated by the superoperator \mathcal{W} given by

$$\dot{\rho}_S = \mathcal{W}\rho_S \quad (48)$$

The superoperator has two parts: coherent evolution \mathcal{W}_0 and dissipator \mathcal{W}_d . The coherent evolution is the unitary part defined by the von Neumann equation:

$$\mathcal{W}_0\rho_S = i[\rho_S, H_S] \quad (49)$$

where H_S is the system Hamiltonian defined in (8). The dissipator originates from the interaction between the system and the environments, defined in (18). The time evolution operator to the zeroth order of coupling is the superoperator with coherent evolution only.

We choose the standard dichotomic observable

$$Q = \sigma_{z,1} = (|g\rangle\langle g| - |e\rangle\langle e|) \otimes \mathbb{1}_2 \quad (50)$$

to testify LGI. Here $\mathbb{1}_2$ is identity operator. In the energy basis (10), the observable Q has the matrix form

$$Q = \begin{pmatrix} 1 & 0 & 0 & 0 \\ 0 & -\cos \theta & \sin \theta & 0 \\ 0 & \sin \theta & \cos \theta & 0 \\ 0 & 0 & 0 & -1 \end{pmatrix} \quad (51)$$

with θ defined in (11). Although we can optimize the choice of local observables in order to maximize $\mathcal{I}_{\max}(\rho^{\text{ss}})$ [26], the observable Q in (50) is a natural description of local realism of the qubit system.

In zeroth order of coupling J , correlation function $C_q(t)$ defined in (3) is obtained from the coherent evolution \mathcal{W}_0 . We have

$$C_q^{(0)}(t, \rho) = 1 - (1 - \cos(\Omega t)) \sin^2 \theta (\rho_{22} + \rho_{33}) \quad (52)$$

The frequency Ω is defined in (34). The zeroth order correlation function $C_q^{(0)}(t)$ oscillates with the period $\Omega/2\pi$. We have the perfect oscillation (without decay) because the coupling to the environments is turned off. If we turn off the inter-qubit coupling, i.e., $\lambda = 0$, which means the two-qubit systems are decoupled, we have

$$C_q^{(0)}(t, \rho(\lambda = 0)) = 1 \quad (53)$$

We have the perfect correlation because observable Q commutes with H_S when $\lambda = 0$.

Given by the zeroth-order correlation function $C_q^{(0)}(t, \rho)$, LGI function defined in (4) has the form

$$\begin{aligned} \mathcal{I}^{(0)}(t, \rho^{\text{ss}}) &= \\ &1 + (2 \cos(\Omega t) - \cos(2\Omega t) - 1) \sin^2 \theta (\rho_{22}^{\text{ss}} + \rho_{33}^{\text{ss}}) \end{aligned} \quad (54)$$

We have the first maximal value when $t = \pi/3\Omega$, which gives

$$\mathcal{I}_{\max}(\rho^{\text{ss}}) = \frac{1}{2} \sin^2 \theta (\rho_{22}^{\text{ss}} + \rho_{33}^{\text{ss}}) \quad (55)$$

The classical description of LGI function defined in (2) is bounded by 1. We will have $\mathcal{I}(t, \rho^{\text{ss}}) > 1$ during the time $0 < t < \pi/(2\Omega)$ and $(3/2 + 2k)\pi/\Omega < t < (5/2 + 2k)\pi/\Omega$ with $k = 0, 1, \dots$, as long as we have (nonzero) steady state population $(\rho_{22} + \rho_{33})$ and nonzero inter-qubit coupling $\lambda \neq 0$.

Note that only populations ρ_{22} and ρ_{33} contribute to the violation of LGI, because states $|1\rangle$ and $|4\rangle$ defined in (10) are product states and their evolution admits classical descriptions. Also when $\lambda = 0$ (the two-qubit systems are decoupled), eigenstates are all product states and the time evolution operator for the local states are diagonalized (classical probability descriptions). When we have two identical qubits ($\omega_1 = \omega_2$), if the population for state $|2\rangle$ and $|3\rangle$ is maximal, i.e., $\rho_{22}^{ss} + \rho_{33}^{ss} = 1$, the violation of LGI is saturated [9]. Notice that the symmetric qubits will have eigenstates $|2\rangle$ and $|3\rangle$ as maximal entangled two qubit states (Bell-like states). Therefore, we can see that the coherent evolution of the spatial maximal entangled states also has the maximal violation of LGI. Then it is reasonable to view the maximum of the LGI function defined in (5) as a quantitative measure for quantum temporal correlation.

The zeroth order of LGI function $\mathcal{I}^{(0)}(t, \rho^{ss})$ in (54) oscillates without decay, which implies the information of the system is preserved (LGI violation can occur at any long time interval between the two measurements). See FIG. 1 for comparison between the zeroth-order, the first-order and the numerical LGI functions. The physical meaning of the zeroth order of LGI function $\mathcal{I}^{(0)}(t, \rho^{ss})$ is that the steady state (coupled with the environments) evolves coherently (decoupled from the environments) after the first measurement. The zeroth order $\mathcal{I}^{(0)}(t, \rho^{ss})$ has the same form both in equilibrium and nonequilibrium cases (and the same for Bosonic and Fermionic baths), being different only in the steady state terms $\rho_{22}^{ss} + \rho_{33}^{ss}$.

B. Leggett-Garg Inequality in the First Order Coupling

The superoperator \mathcal{W} in (48) characterizing the time evolution of the system has the matrix form \mathcal{M} (Liouville space), see (23). Then we have the time evolution:

$$|\rho_S(t)\rangle = e^{\mathcal{M}t}|\rho_S\rangle \quad (56)$$

Note that the evolution operator $e^{\mathcal{M}t}$ is defined in the energy basis. The analytical form of $e^{\mathcal{M}t}$ is complicated, even when the matrix \mathcal{M} can be diagonalized. Note that the real part of \mathcal{M} is related to the overall coupling constant J and the imaginary part of \mathcal{M} is related to the coherent oscillation only, namely we have

$$\mathcal{M} = \mathcal{M}_0 + \mathcal{M}_J \quad (57)$$

with

$$\mathcal{M}_J = \text{Re}\mathcal{M}, \quad \mathcal{M}_0 = i\text{Im}\mathcal{M}, \quad (58)$$

see the matrix elements of \mathcal{M} in (A1)-(A14).

We can apply the Zassenhaus formula [72] in the first order of the coupling constant J :

$$e^{\mathcal{M}t} = \left(\mathbb{1} + \sum_{n=1}^{\infty} \frac{t^n}{n!} \mathcal{L}_{\mathcal{M}_0}^{n-1} \mathcal{M}_J + \mathcal{O}(\mathcal{M}_J^2) \right) e^{\mathcal{M}_0 t} \quad (59)$$

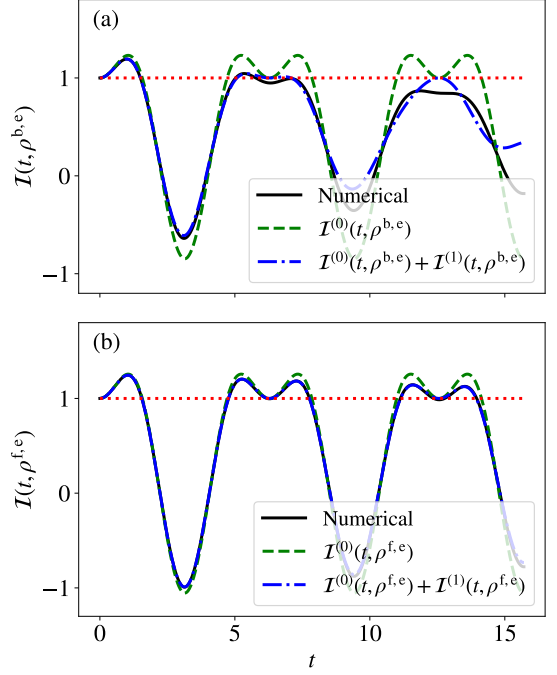


FIG. 1. LGI function $\mathcal{I}(t, \rho^{ss})$ defined in (4) for two qubit system coupled with two (a) Bosonic or (b) Fermionic baths. Parameters are set as $\omega_1 = \omega_2 = \lambda = 1$ and $J = 0.005$. Solid line is numerical results based on the Redfield equation (17); dashed line is the zeroth order J of LGI function $\mathcal{I}^{(0)}(t, \rho^{ss})$ in (54); dot-dashed line is up to the first order J of LGI function: $\mathcal{I}^{(0)}(t, \rho^{ss}) + \mathcal{I}^{(1)}(t, \rho^{ss})$; analytical expression of $\mathcal{I}^{(1)}(t, \rho^{b,e})$ and $\mathcal{I}^{(1)}(t, \rho^{f,e})$ can be found in (64) and (70) respectively. Above the red line suggests the violation of LGI (in classical description). (a). Two Bosonic baths with the same temperature $T = 1.5$. (b). Two Fermionic bath with the same chemical potentials $\mu = 1$ and temperature $T = 1.5$.

where \mathcal{L} is the commutator operator

$$\mathcal{L}_{\mathcal{M}_0} \mathcal{M}_J = [\mathcal{M}_0, \mathcal{M}_J] \quad (60)$$

Evolution $\exp(\mathcal{M}_0 t)$ is the coherent part discussed before. The above expansion is based on small coupling J . More specifically, the matrix elements of $\mathcal{M}_J t$ should be much less than 1, formally

$$t J n_l(\omega'_{1,2}) \ll 1 \quad (61)$$

It suggests that we have good agreement for the first order LGI function when t is small, see FIG. 1. The approximation condition in (61) requires low temperature: $T < \omega'_{1,2}$ for Bosonic reservoirs. Since the mean particle occupation number $n_l(\omega'_{1,2})$ is bounded in Fermionic baths due to the exclusion principle, we have the approximation condition $t \ll 1/J$. The bounded mean particle occupation number in Fermionic cases also suggest we have better approximation in first order LGI function, see FIG. 1. The systems are supposed to be “classical” and LGI is preserved when the environments are at high temperatures. We will numerically check that LGI is not violated in the high temperature regime.

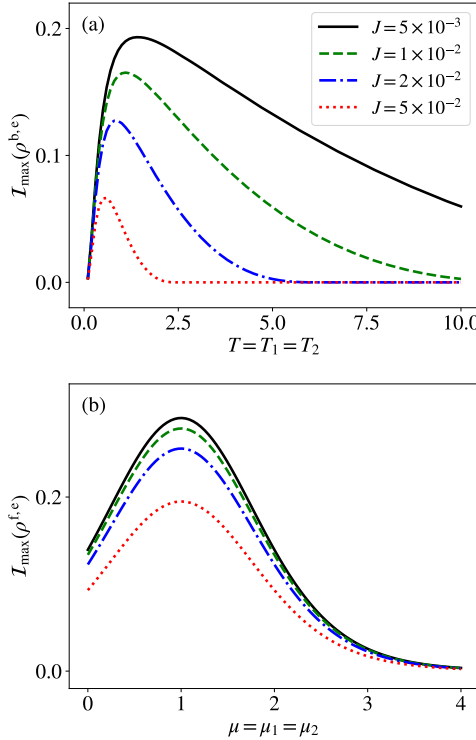


FIG. 2. MLGI $I_{\max}(\rho^{\text{b},\text{e}})$ defined in (5) in terms of system-bath coupling J and (a) equilibrium temperature for Bosonic bath and (b) equilibrium chemical potential for Fermionic bath with temperature $T = 0.5$. Parameters are set as $\omega_1 = \omega_2 = \lambda = 1$.

1. Equilibrium Bosonic Bath

Equilibrium steady state does not have coherence in energy basis, i.e., the population space and coherence space are decoupled in the Blch-Redfield equation, see (17). However, coherence in localized state representation always survives if we have non-vanishing inter-qubit coupling λ . Matrix elements of \mathcal{M} in (23) is block diagonalized in the energy basis. Moreover, we can check that the real (dissipation) and imaginary part (coherent evolution) in matrix \mathcal{M} commute, i.e.,

$$[\mathcal{M}_0, \mathcal{M}_J] = 0, \quad \text{if } T_1 = T_2 \quad (62)$$

The expansion of the exponential (59) is then greatly simplified as:

$$e^{\mathcal{M}t} = (\mathbb{1} + \mathcal{M}_J t + \mathcal{O}(\mathcal{M}_J)) e^{\mathcal{M}_0 t}, \quad \text{if } T_1 = T_2 \quad (63)$$

The above relation also holds for equilibrium Fermionic bath ($\mu_1 = \mu_2 = \mu$). It is straightforward to calculate the first order J correction to the LGI function:

$$\begin{aligned} \mathcal{I}^{(1)}(t, \rho^{\text{b},\text{e}}) &= 4tJ \sin^2 \theta(\rho_{22}^{\text{b},\text{e}} + \rho_{33}^{\text{b},\text{e}}) (n(\omega'_1) + n(\omega'_2) + 1) \\ &\times (\cos(2\Omega t) - \cos(\Omega t)) \end{aligned} \quad (64)$$

with notation $n(\omega'_{1,2}) = n_1(\omega'_{1,2}) = n_2(\omega'_{1,2})$ (because we have $T_1 = T_2 = T$). We omit the superscript “ss” for simplicity.

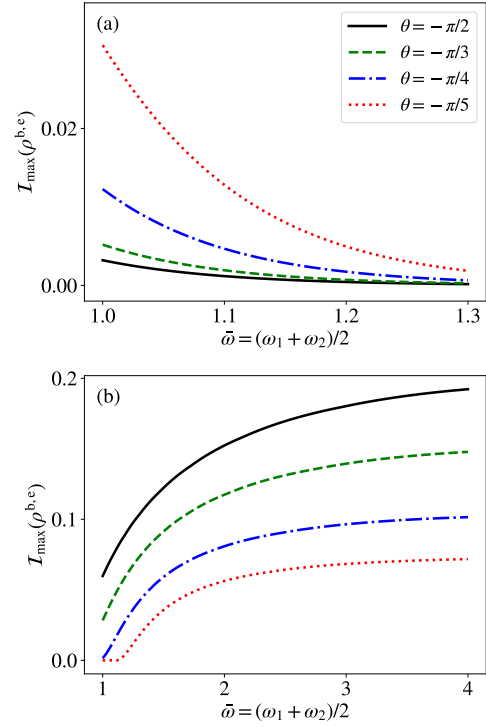


FIG. 3. MLGI $I_{\max}(\rho^{\text{b},\text{e}})$ defined in (5) of equilibrium Bosonic bath in terms of mean energy splitting $\bar{\omega}$ and detuning angle (with fixed $\lambda = 1$) characterizing the asymmetry of the two qubit system. The coupling is set as $J = 0.005$. The two Bosonic bath have the same (a) temperatures $T = 0.1$ or (b) temperatures $T = 10$.

The first order correction $\mathcal{I}^{(1)}(t, \rho^{\text{b},\text{e}})$ is proportional to $tJn(\omega'_{1,2})$ and oscillates in period $2\pi/\Omega$. We know that the zero-th order LGI function in (54) has the maximum at $(1/(3\Omega) + 2n)\pi$ and $(5/(3\Omega) + 2n)\pi$ with integer number $n \geq 0$. We can check that those extremal points always give negative $\mathcal{I}^{(1)}(t, \rho^{\text{b},\text{e}})$ in (64). Also note that $\mathcal{I}^{(1)}(t, \rho^{\text{b},\text{e}})$ linearly increases with time t . Therefore, LGI function is decaying due to incoherent evolution (system coupled with the environments). After a threshold time (the interval time between two measurements), the inequality will not be violated and the system admits classical description between two measurements. The first order correction is proportional to $\sin^2 \theta$ and the population sum $\rho_{22}^{\text{b},\text{e}} + \rho_{33}^{\text{b},\text{e}}$. It is interesting to see that when $\lambda = 0$ or $\rho_{22}^{\text{b},\text{e}} + \rho_{33}^{\text{b},\text{e}} = 0$, the first order correction is also zero. Although the two qubits are decoupled $\lambda = 0$, LGI is still expected to decay due to coupling with the environments (information leaked into environments). However such effects are beyond first order J , which means that coupled two qubit system is more easily affected by the environments (more fragile than the local states). See FIG. 1 for the comparison among numerical calculations, its zeroth order and first order of LGI function $\mathcal{I}(t, \rho^{\text{e},\text{b}})$.

The zero-th order of LGI function $\mathcal{I}^{(0)}(t, \rho^{\text{b},\text{e}})$ in (54) has the maximum at $t = \pi/(3\Omega)$. We can approximate the first order of MLGI $I_{\max}(\rho^{\text{b},\text{e}})$ defined in (5) by

$$\mathcal{I}_{\max}^{(1)}(\rho^{\text{b},\text{e}}) \approx \mathcal{I}^{(1)}(t = \pi/(3\Omega), \rho^{\text{b},\text{e}}), \quad (65)$$

which gives

$$\begin{aligned} \mathcal{I}_{\max}^{(1)}(\rho^{\text{b,e}}) = & \\ & -\frac{4\pi J}{3\Omega} \sin^2 \theta (\rho_{22}^{\text{b,e}} + \rho_{33}^{\text{b,e}}) (n(\omega'_1) + n(\omega'_2) + 1) \end{aligned} \quad (66)$$

The first order $\mathcal{I}_{\max}^{(1)}(\rho^{\text{b,e}})$ is always negative irrespective to the bath parameters. Increasing the coupling J will always decrease MLGI⁽¹⁾, namely moving the system towards the classical description.

To better see how the temperature T affects $\mathcal{I}_{\max}^{(1)}(\rho^{\text{b,e}})$, we can approximate the mean particle occupation number as

$$n(\omega'_{1,2}) \approx e^{-\omega'_{1,2}/T} \quad (67)$$

if $T \ll \omega'_{1,2}$. Then we have

$$\mathcal{I}_{\max}^{(0)}(\rho^{\text{b,e}}) + \mathcal{I}_{\max}^{(1)}(\rho^{\text{b,e}}) \approx \alpha \sin^2 \theta \left(\frac{1}{2} - \frac{4\pi J}{3\Omega} \right) \quad (68)$$

with

$$\alpha = 2e^{-\bar{\omega}/T} \cosh \left(\frac{\Omega}{2T} \right) \quad (69)$$

Here the parameter α has the physical meaning: proportional to the population term, i.e., $\alpha \propto (\rho_{22}^{\text{b,e}} + \rho_{33}^{\text{b,e}})$. Increasing the temperature T (when $T \ll \omega'_{1,2}$) gives the MLGI enhancement. Approximately zero temperature does not have LGI violation because the system will always be in the ground state $|1\rangle$, and the time evolution of the ground state is trivial. *The population of excited states is the key for LGI violation.* If we do not have the non-local ground state, but have non-local excited state, then the bath temperature, which gives the excitation, is beneficial for enhancing the LGI violation.

High temperature environment deteriorates the quantumness of the system and LGI is preserved. For example, if the temperature is around $T \sim 10\omega'_{1,2}$ (approximation condition in (61) can still be valid), this gives almost even distribution in population space, see (41). Further increasing the temperature does not increase the population sum $\rho_{22}^{\text{b,e}} + \rho_{33}^{\text{b,e}}$. However, increasing the temperature (when $T \sim 10\omega'_{1,2}$) will dramatically increase $n(\omega'_1) + n(\omega'_2)$ and therefore the first order correction $\mathcal{I}_{\max}^{(1)}(\rho^{\text{b,e}})$ in (66) will decrease. At intermediate temperature $T \sim \omega'_{1,2}$, MLGI $\mathcal{I}_{\max}(\rho^{\text{b,e}})$ is compromised between the non-local state population and decoherence. We can numerically explore the non-monotonic relation between MLGI $\mathcal{I}_{\max}(\rho^{\text{b,e}})$ and temperature T , see FIG. 2. We can also check the monotonic relation between MLGI $\mathcal{I}_{\max}(\rho^{\text{b,e}})$ and coupling J , see FIG. 2. Stronger coupling J leads to that the environment destroys the coherence (in energy basis) faster. Increasing the temperature can lead to both the excited non-local states and the decoherence effect, giving rise to non-monotonic behavior.

When the two qubits have different transition frequency $\Delta\omega \neq 0$, the eigenstates $|2\rangle$ and $|3\rangle$ (defined in (10)) will become less entangled. The detuning angle θ in (11) is $\theta = -\pi/2$ when $\Delta\omega = 0$. Turning off the coupling of the

two qubit systems ($\lambda = 0$) leads to the classical descriptions (probability rate equation) of the time evolution of the system. Inter-qubit coupling strength λ has the monotonic relation with MLGI $\mathcal{I}_{\max}(\rho^{\text{b,e}})$ (smaller λ gives smaller $\mathcal{I}_{\max}(\rho^{\text{b,e}})$). However, $\mathcal{I}_{\max}(\rho^{\text{b,e}})$ does not have monotonic relation with $\Delta\omega$ (changing θ with fixed λ), see FIG. 3.

Recall that in low temperature regime ($T \ll \omega'_{1,2}$), MLGI $\mathcal{I}_{\max}(\rho^{\text{b,e}})$ up to the first order of J has the form (68), where α is proportional to the population term. If we increase the transition frequency difference $\Delta\omega$ (with fixed average $\bar{\omega}$), the oscillation frequency Ω in (34) will increase. Then α is larger with larger Ω . In other words, we can increase the population sum $\rho_{22}^{\text{b,e}} + \rho_{33}^{\text{b,e}}$ by increasing the frequency difference $\Delta\omega$. In a more intuitive understanding, if the ground state is dominated, population $\rho_{22}^{\text{b,e}}$ will increase if we lower the energy level of state $|2\rangle$. Note that the eigenstate $|2\rangle$ has the energy $\omega'_1 = \bar{\omega} - \sqrt{\Delta\omega^2 + \lambda^2}/2$. Besides, we can enhance MLGI $\mathcal{I}_{\max}(\rho^{\text{b,e}})$ in the low temperature regime by lowering the average frequencies $\bar{\omega}$ (which is physically equivalent to increasing the equilibrium temperature of the two baths). See the numerical results in FIG. 3 which is consistent with the analytical arguments.

If the equilibrium temperature T is high ($T \gg \omega'_{1,2}$), population sum $\rho_{22}^{\text{b,e}} + \rho_{33}^{\text{b,e}}$ is saturated around 1/2. The overall factor $\sin^2 \theta$ is dominated in $\mathcal{I}_{\max}(\rho^{\text{b,e}})$ in (66). Decreasing $\Delta\omega$ with fixed λ or increasing λ with fixed $\Delta\omega$ will both enhance MLGI $\mathcal{I}_{\max}(\rho^{\text{b,e}})$. The more physical intuitive explanation is that the maximal entangled nonlocal states violate the local realism maximally. Therefore, we want both qubits to have the same frequencies in order to form the Bell-like eigenstates. Also in high temperature case, lowing temperature is beneficial to test LGI violation, see FIG. 2. Then we can enhance MLGI $\mathcal{I}_{\max}(\rho^{\text{b,e}})$ by increasing the mean energy splitting $\bar{\omega}$. We numerically checked the above arguments, see FIG. 3.

2. Equilibrium Fermionic Bath

We study the LGI violation in two-qubit system (toy model of double quantum dots) coupled with equilibrium Fermionic environments. We limit in the low temperature regimes in the following parts (for the Fermionic environments). Similar to the equilibrium Bosonic case, population space and coherent space in energy basis are decoupled in Bloch-Redfield equation (17), which implies the commutative relation (62). Note that the time evolution matrix \mathcal{M} defined in (23) has different matrix elements for Bosonic and Fermionic setups, because of difference in Boson-Einstein distribution and Fermi-Dirac distribution.

In the first order coupling constant J , LGI function (4) has the form

$$\mathcal{I}^{(1)}(t, \rho^{\text{f,e}}) = 4tJ \sin^2 \theta (\rho_{22}^{\text{f,e}} + \rho_{33}^{\text{f,e}}) (\cos(2\Omega t) - \cos(\Omega t)) \quad (70)$$

The steady state $\rho^{\text{f,e}}$ has the form in (45). And we approximate the first order MLGI function $\mathcal{I}_{\max}(\rho^{\text{f,e}})$ defined in (5) by (the zeroth order of LGI function $\mathcal{I}_{\max}^{(0)}(\rho^{\text{f,e}})$ has a maximum at $t =$

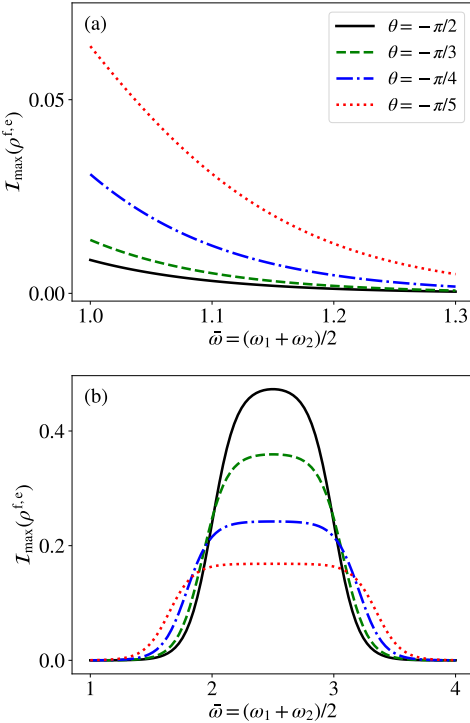


FIG. 4. MLGI $I_{\max}(\rho^{b,e})$ defined in (5) of equilibrium Fermionic bath in terms of mean energy splitting $\bar{\omega}$ and detuning angle (with fixed $\lambda = 1$) characterizing the asymmetric of the two qubit system. The coupling is set as $J = 0.005$. And the temperature is $T = 0.1$. The two Fermionic bath has the same (a) chemical potential $\mu = 0.1$ or (b) $\mu = 2.5$.

$\pi/(3\Omega))$

$$\begin{aligned} I_{\max}^{(1)}(\rho^{f,e}) &\approx I^{(1)}(t = \pi/(3\Omega), \rho^{f,e}) \\ &= -\frac{4\pi J}{3\Omega} \sin^2 \theta (\rho_{22}^{f,e} + \rho_{33}^{f,e}) \end{aligned} \quad (71)$$

The first order correction $I_{\max}^{(1)}(\rho^{f,e})$ is always negative. Both the zeroth and the first order of MLGI function are even functions of $\bar{\omega} - \mu$, indicating local minimum or maximum at $\mu = \bar{\omega}$. If $T \ll \bar{\omega}$ (low temperature regime), we have the population sum

$$\rho_{22}^{f,e} + \rho_{33}^{f,e} \approx \frac{1}{\exp\left(\frac{2|\bar{\omega} - \mu| - \Omega}{2T}\right) + 1} \quad (72)$$

The resonant point $\bar{\omega} = \mu$ gives the maximal population of the nonlocal states (eigenstates $|2\rangle$ and $|3\rangle$ are entangled states). The ground state has the particle occupation number 0; the first and the second excited state have the particle occupation number 1 and the highest excited state has the particle occupation number 2. At the resonant point $\bar{\omega} = \mu$, the system is driven into the first and the second excited states. Therefore the zeroth order of MLGI function (55) has the global maximum at $\bar{\omega} = \mu$. Low chemical potential reservoir can not pump electrons into dots (state $|1\rangle$); But high chemical potential reservoir makes all dots occupied (state $|4\rangle$). Both states

$|1\rangle$ and $|4\rangle$ admit local realism descriptions. See FIG. 2 for the numerical results of MLGI $I_{\max}(\rho^{f,e})$ in terms of the coupling constant and the chemical potential μ .

When the ground state is dominated (two empty sites), we can increase the population sum of the first and the second excited states by lowering the mean energy splitting $\bar{\omega}$ or increasing the local energy level difference $\Delta\omega$. We can reversely argue the high chemical potential case. The above arguments are similar to the Bosonic case. Consider the intermediate chemical potential regime $\mu \sim \bar{\omega}$: population sum of the first and the second excited state is almost saturated. Then changing the energy difference $\Delta\omega$ does not affect the population sum of states $|2\rangle$ and $|3\rangle$. However, states $|2\rangle$ and $|3\rangle$ will become less entangled (more local). Then we always have larger MLGI function $I_{\max}(\rho^{b,e})$ in (5) when $\theta = -\pi/2$, see the numerical results in FIG. 4. On the contrary, away from the resonant point $\mu \sim \bar{\omega}$, we always have MLGI $I_{\max}(\rho^{b,e})$ enhancement by increasing the local energy level difference $\Delta\omega$, although we have less entangled excited states.

V. LEGGET-GARG INEQUALITY VIOLATION IN NONEQUILIBRIUM CASE

In this section, we explore how the nonequilibrium condition, characterized by temperature difference $\Delta T = T_2 - T_1$ for Bosonic bath or chemical potential difference $\Delta\mu = \mu_2 - \mu_1$ for Fermionic bath, contributes to the violation of LGI. The nonequilibrium environments suggests the heat or particle current flowing through the system [31, 48, 50, 52, 54, 56, 58, 59, 62]. Consequently, there will be nonzero thermodynamic dissipation characterized by the entropy production rate [48, 58]. Firstly, we show that the heat or particle current and entropy production rate through the system increases monotonically in terms of the environment bias (temperature difference ΔT or chemical potential difference $\Delta\mu$). Then analytically, we derive the LGI function $I(t, \rho^{ss})$ in (4) and MLGI function $I_{\max}(\rho^{ss})$ in (5) in the first order of coupling constant J (approximation valid by the condition (61)) in the nonequilibrium cases. We numerically check the analytical results and numerically explore the relative high temperature cases.

A. Heat/Particle Current and Entropy Production Rate

When the system reaches steady state (under nonequilibrium environments), there is a constant heat or particle current flowing through the system (from high temperature or chemical potential bath to low temperature or chemical potential bath). The heat current is characterized by the energy change with the two environments. We have

$$\text{Tr}(\dot{\rho}H_S) = \sum_{l=1}^2 I_l^b \quad (73)$$

where I_l^b with $l = 1, 2$ are the heat currents through the bath 1 or 2. Superscript b reminds that we have Bosonic environments. Positive I_l means that the heat current is flowing into

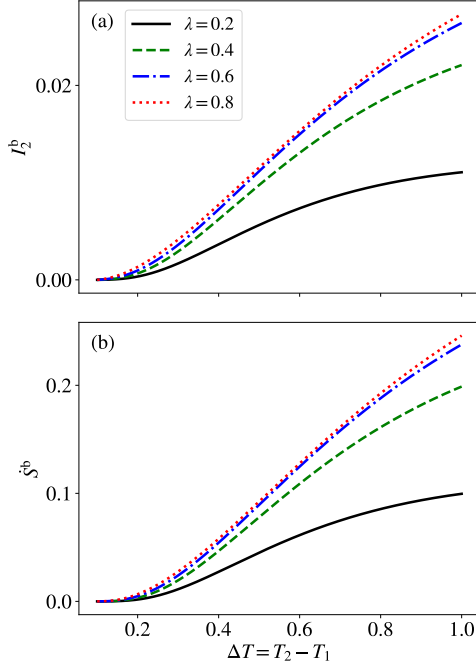


FIG. 5. (a) Heat current I_2^b defined in (74) and (b) entropy production rate \dot{S}^b defined in (76) at steady state in terms of nonequilibrium condition $\Delta T = T_2 - T_1$ with fixed $T_1 = 0.1$. Parameters are set as $\bar{\omega} = 1$, $\theta = -\pi/2$ and $J = 0.1$.

the system. According to the Bloch-Redfield equation (17), the heat currents are related with dissipators:

$$I_l^b = \text{Tr}(\mathcal{D}_l[\rho]H_S) \quad (74)$$

Steady state means $\text{Tr}(\dot{\rho}^{\text{ss}} H_S) = 0$. Therefore the two currents have the same magnitude but different directions:

$$I_1^b + I_2^b = 0 \quad (75)$$

If $T_2 > T_1$, we have $I_2^b > 0$ and $I_1^b < 0$.

Given by the analytical results of nonequilibrium steady state ρ^b , see (32a)-(32d) and (37), we can find the steady state heat current. We give the analytical steady state heat current in Appendix C. We plot the heat current I_2^b in terms of nonequilibrium condition $\Delta T = T_2 - T_1$ (with fixed T_1) in FIG. 5. The current magnitude increases monotonically with the temperature bias ΔT . The inter qubit coupling (characterized by strength λ) plays important role in heat transport [50, 59, 62]. As $\lambda = 0$, the two-qubit system is decoupled and the two environments are separated. No heat current flows through the system. Increasing the inter-qubit coupling strength λ can enhance the heat flow, see FIG. 5.

Since the two reservoirs are assumed to be infinitely large compared with system, the steady state can be maintained for a very long time. We assume that the equilibrium temperatures of the two baths are always constant. The nonzero constant heat transfer at steady state implies that we have constant entropy production rate defined as

$$\dot{S}^b = -\frac{I_1^b}{T_1} - \frac{I_2^b}{T_2} = I_2^b \left(\frac{1}{T_1} - \frac{1}{T_2} \right) \quad (76)$$

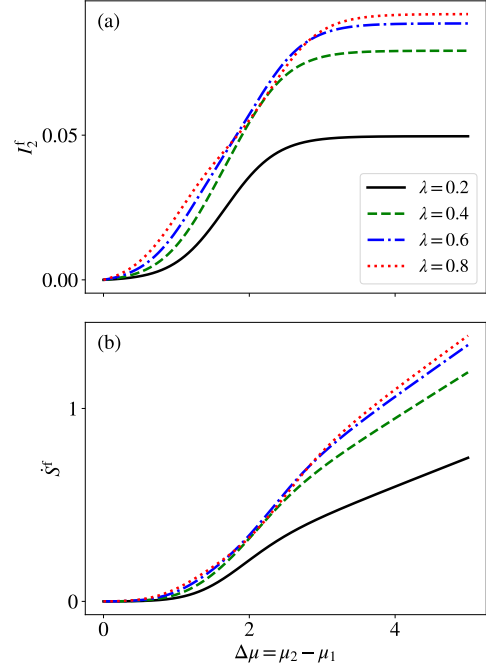


FIG. 6. (a) Particle current I_2^f defined in (78) and (b) entropy production rate \dot{S}^f defined in (81) at steady state in terms of nonequilibrium condition $\Delta \mu = \mu_2 - \mu_1$ with fixed $\mu_1 = 0$. The two baths have the same temperature $T_1 = T_2 = 0.2$. Parameters are set as $\bar{\omega} = 1$, $\theta = -\pi/2$ and $J = 0.1$.

Same magnitude $|\Delta T|$ gives the same entropy production rate $\dot{S}^b > 0$. The entropy production rate also monotonically increases with nonequilibrium condition, see FIG. 5. The stronger inter-qubit coupling gives larger entropy production rate, since we have larger steady state heat current. At far from equilibrium case, for example $T_1 \rightarrow 0$ and $T_2 \rightarrow \infty$, the entropy production rate is proportional to the heat current:

$$\dot{S}^b \approx \frac{I_2^b}{T_1} \quad (77)$$

Nonequilibrium Fermionic environments suggest particle current flowing through the system. We can keep track of the particle number change in the system to reveal the particle current. Similarly with heat current, we define the particle current with respect to the two baths as

$$I_l^f = \text{Tr}(\mathcal{D}_l[\rho]N_S) \quad (78)$$

with particle operator N_S in energy basis $N_S = |2\rangle\langle 2| + |3\rangle\langle 3| + 2|4\rangle\langle 4|$. Steady state gives

$$I_1^f + I_2^f = 0 \quad (79)$$

Positive current means that electron flows into the system. The analytical expression of the particle current is given in Appendix C. We plot the particle current in terms of the chemical potential difference $\Delta \mu = \mu_2 - \mu_1$ with fixed μ_1 in FIG. 6. Due to the Pauli exclusion principle (particle occupation number $n(\omega)$ (21) is less than 1), particle current becomes

saturated when we have large chemical potential bias. For example, at relative low temperature regime $T \ll \bar{\omega}$, if $\mu_1 \rightarrow 0$ and $\mu_2 \rightarrow \infty$, we have the particle current

$$I_2^f \approx J(1 + \rho_{23}^f + \rho_{32}^f) = J \left(1 - \frac{1}{1 + (\lambda/2J)^2} \right) \quad (80)$$

assuming $\omega_1 = \omega_2$ and constant symmetric coupling spectral J (29). The current is proportional to the coherence in the energy basis. The particle current is bounded by J . Increasing the inter-qubit coupling gives larger particle current as expected, see FIG. 6.

The two Fermionic environments are characterized by the (different) equilibrium chemical potentials and the temperatures respectively at the steady state. The entropy production rate of the environments is

$$\dot{S}^f = \frac{\mu_1 I_1^f}{T} + \frac{\mu_2 I_2^f}{T} = \frac{\mu_2 - \mu_1}{T} I_2^f \quad (81)$$

Here for simplicity, we assume the same temperatures $T = T_1 = T_2$ of the two baths to explore how chemical potential difference influences the dynamics and thermodynamic dissipation. At far from equilibrium case, the particle current is saturated. Therefore the entropy production rate increases lin-

early with the nonequilibrium condition $\Delta\mu = \mu_2 - \mu_1$, see FIG. 6.

B. MLGI Enhanced by the Nonequilibrium Bosonic Environments

In Liouville space, the time evolution operator is given by $e^{\mathcal{M}t}$ with the matrix elements in (A1)-(A14), see (56). When we have nonzero nonequilibrium condition ΔT , the density matrix in population space and coherence space is not decoupled, unlike the equilibrium case. Therefore, steady state coherence in the eigenstate representation can survive in nonequilibrium environments [49, 50, 59]. The time evolution matrix \mathcal{M} can be decomposed into coherent evolution part \mathcal{M}_0 and dissipation part \mathcal{M}_J , see (57). These two parts do not commute in nonequilibrium cases. As a result, the Zassenhaus formula in the first order \mathcal{M}_J in (59) will have summation for infinite series. Fortunately, the sum has the closed form due to the simple structure of \mathcal{M}_0 . For simplicity, we consider symmetric qubit $\omega_1 = \omega_2$ in the following analytical study. We obtain the first order LGI function $\mathcal{I}(t, \rho^b)$ with the nonequilibrium corrections:

$$\mathcal{I}^{(1)}(t, \rho^b) = 4tJ(\rho_{22}^b + \rho_{33}^b)(\tilde{n}_1 + \tilde{n}_2 + 1)(\cos(2\lambda t) - \cos(\lambda t)) + \frac{2J}{\lambda}(\Delta n_1 + \Delta n_2)(\sin(2\lambda t) - 2\sin(\lambda t)) \quad (82)$$

The steady state ρ^b has the analytical solution in (32a)-(32d). The first term is the equilibrium correction (with $\sin^2 \theta = 1$), see (64).

To better see how the nonequilibrium condition affects the LGI violation, we approximate the MLGI $\mathcal{I}_{\max}(\rho^b)$ as (same as the equilibrium case):

$$\begin{aligned} \mathcal{I}_{\max}^{(1)}(\rho^b) &\approx \mathcal{I}^{(1)}(t = \pi/(3\lambda), \rho^b) \\ &= -\frac{4\pi J}{3\lambda}(\rho_{22}^b + \rho_{33}^b) - \frac{\sqrt{3}J}{\lambda}(\Delta n_1 + \Delta n_2) \end{aligned} \quad (83)$$

with $\lambda \neq 0$. Note that $\lambda = 0$ (decoupled two qubit system) is trivial for LGI violation. The first order MLGI $\mathcal{I}_{\max}^{(1)}(\rho^b)$ is always negative irrespect to either $T_2 > T_1$ or $T_1 < T_2$. The second term in $\mathcal{I}_{\max}^{(1)}(\rho^b)$ is the corresponding nonequilibrium correction. Note that we also have nonequilibrium corrections in steady state solution (32a)-(32d), which is proportional to J^2 order.

The nonequilibrium correction in $\mathcal{I}_{\max}^{(1)}(\rho^b)$ is not a symmetric function of temperatures T_1 and T_2 . Simple argument shows that $\Delta n_{1,2} < 0$ with $T_2 > T_1$. Therefore we can expect MLGI function $\mathcal{I}_{\max}^{(1)}(\rho^b)$ enhancement with $T_2 > T_1$. The two-qubit system is symmetric with T_1 and T_2 if the two qubits are identical ($\omega_1 = \omega_2$). The asymmetric LGI function and MLGI function comes from choosing the local observable $\sigma_{z,1}$ for qubit 1 only. If we tune the two-qubit coupling λ to

be small, qubit 2 coupled bath with temperature T_2 becomes another environment in terms of qubit 1. If bath 1 has high temperature, then qubit 1 becomes classical.

In the equilibrium scenario, MLGI function $\mathcal{I}_{\max}(\rho^{b,e})$ has none-monotonic relationship with the temperatures $T = T_1 = T_2$, see FIG. 2, resulting from the competition between nonlocal state population and the decoherence effects on the system. In the following, we fix the mean temperature and study the relationship between the MLGI function $\mathcal{I}_{\max}(\rho^b)$ and nonequilibrium condition $\Delta T = T_2 - T_1$. If we have relative low mean temperature ($T_m \ll \bar{\omega}$ with $T_m = 1/2(T_1 + T_2)$), we get the approximation:

$$\mathcal{I}_{\max}^{(0)}(\rho^b) + \mathcal{I}_{\max}^{(1)}(\rho^b) \approx \alpha' \left(\frac{1}{2} + \frac{J}{\lambda} \left(\pm \sqrt{3} - \frac{4\pi}{3} \right) \right) \quad (84)$$

The plus sign is for $T_2 > T_1$ and minus sign is for $T_2 < T_1$. Parameter α' is defined as

$$\alpha' = e^{-\omega'_1/T_{\text{eff}}} + e^{-\omega'_2/T_{\text{eff}}} \quad (85)$$

with the effective temperature

$$T_{\text{eff}} = 2T_m^2/(2T_m - |\Delta T|) \quad (86)$$

With $\Delta T = 0$, the effective temperature is the equilibrium temperature $T_{\text{eff}} = T_1 = T_2 = T$, and α' is back to the equilibrium parameter α defined in (69). The parameter α' is approximated from the nonlocal state population sum $\rho_{22}^b + \rho_{33}^b$.

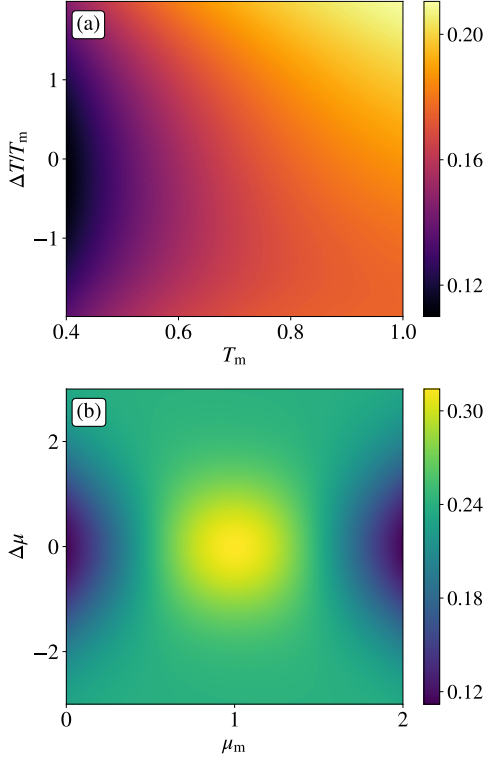


FIG. 7. The phase diagram of MLGI function $\mathcal{I}_{\max}(\rho^{\text{ss}})$ defined in (5) in terms of (a) the mean temperature T_m and the temperature difference $\Delta T = T_2 - T_1$ for the Bosonic bath and (b) the mean chemical potential μ_m and the chemical potential difference $\Delta\mu = \mu_2 - \mu_1$ for the Fermionic bath with $T = 0.4$. Other parameters are set as $\omega_1 = \omega_2 = \lambda = 1$ and $J = 0.005$. Red-based color is for Bosonic environment and green-based color is for Fermionic environment.

We can increase α' by increasing the mean temperature \bar{T} or the temperature difference ΔT . Therefore the increased MLGI function $\mathcal{I}_{\max}(\rho^{\text{b,e}})$ via nonequilibrium condition can be understood as the increasing nonlocal state population. Besides, the temperature difference at $T_2 > T_1$ is more favorable for LGI violation than the temperature difference at $T_2 < T_1$ (magnitude in the order of J).

When the mean temperature is relative large, say $T_m \sim 10\bar{\omega}$, we know that the states are almost evenly distributed i.e., $\rho_{22}^{\text{b}} + \rho_{33}^{\text{b}} \approx 1/2$. Up to the first order J , we have

$$\begin{aligned} \mathcal{I}_{\max}^{(0)}(\rho^{\text{b}}) + \mathcal{I}_{\max}^{(1)}(\rho^{\text{b}}) &\approx \\ \frac{1}{4} + \frac{J}{\lambda} \left(\left(\frac{1}{\omega'_1} + \frac{1}{\omega'_2} \right) \left(\frac{\sqrt{3}}{2} \Delta T - \frac{2\pi}{3} T_m \right) - \frac{2\pi}{3} \right) \end{aligned} \quad (87)$$

We can see that $\Delta T > 0$ can give LGI violation however $\Delta T < 0$ can not. Such asymmetric contribution is beyond Lindblad description [31]. See FIG. 7 for numerical plot.

The nonequilibrium Bosonic environments have the thermodynamic cost characterized by the entropy production rate \dot{S}^{b} defined in (76). We know that the steady state gives the constant entropy production rate which monotonically in-

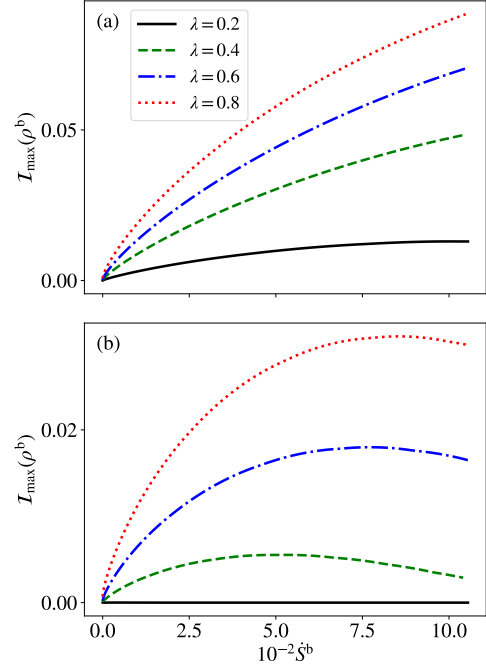


FIG. 8. The MLGI function $\mathcal{I}_{\max}(\rho^{\text{b}})$ defined in (5) in terms of the entropy production rate \dot{S}^{b} defined in (76) with the different inter-qubit coupling strength λ . (a) The temperature T_1 is fixed with $T_1 = 0.1$ or (b) the temperature T_2 is fixed with $T_2 = 0.1$. Other parameters are set as $\omega_1 = \omega_2 = 1$ and $J = 0.05$.

creases with the temperature difference of the two baths, see FIG. 5. The entropy production rate \dot{S}^{b} can be viewed as another thermodynamic nonequilibrium measure, besides the temperature difference ΔT . Suppose that we fix the temperature T_1 at relatively low regime $T_1 \ll \bar{\omega}$. The system will stay at the ground state at the equilibrium case $T_1 = T_2$. Increasing the temperature T_2 will induce the heat current (at steady state) flowing from the bath 2 to the bath 1. And we will have non-zero entropy production rate \dot{S}^{b} generated from the nonequilibrium environments. The consumption in the environments characterized by the entropy production rate \dot{S}^{b} can enhance the LGI violation if the temperature T_1 is relatively low, see FIG. 8. If we fix the temperature T_2 , increasing the temperature T_1 will induce the heat current (at steady state) flowing from the bath 1 to the bath 2. The same magnitude $|\Delta T|$ gives the same entropy production rate. However, we have the stronger enhancement for the MLGI function $\mathcal{I}_{\max}(\rho^{\text{b}})$ consumed by the thermodynamic cost (the nonzero entropy production rate) if $T_1 < T_2$, see FIG. 8. With the same entropy production rate \dot{S}^{b} , larger inter-qubit coupling λ gives larger MLGI function $\mathcal{I}_{\max}(\rho^{\text{b}})$ either $T_1 > T_2$ or $T_1 < T_2$. In other words, we have more efficient thermodynamic cost (to enhance the LGI violations) if we have stronger inter-qubit coupling λ . Intuitively, stronger inter-qubit coupling λ gives more population on the first excited state $|2\rangle$, which is nonlocal.

Detuning the qubit frequency $\Delta\omega$ can increase MLGI function $\mathcal{I}_{\max}(\rho^{\text{b,e}})$ (with equilibrium environments) if the temper-

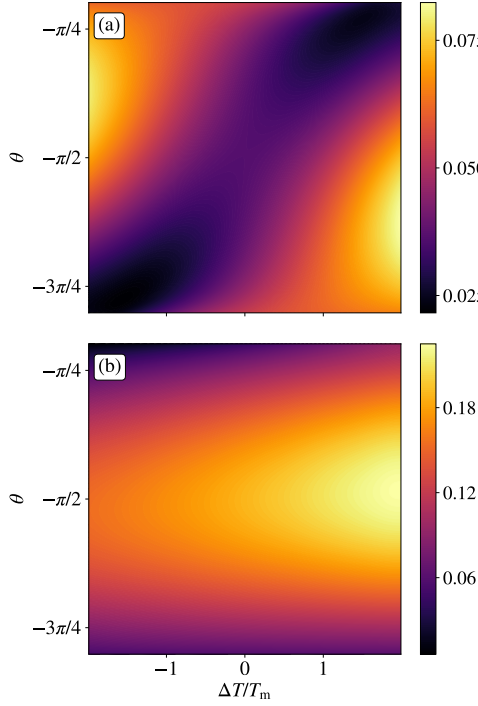


FIG. 9. The MLGI function $\mathcal{I}_{\max}(\rho^{\text{ss}})$ defined in (5) in terms of the nonequilibrium condition $\Delta T = T_2 - T_1$ and the detuning angle θ defined in (11) with fixed $\lambda = 1$. (a) Low mean temperature $T_m = 0.2$ and (b) High mean temperature $T_m = 2$. Other parameters are set as $\bar{\omega} = 1$ and $J = 0.005$.

ature $T = T_1 = T_2$ is relatively low, see FIG. 3. The relationship between the frequency difference $\Delta\omega$ and MLGI function $\mathcal{I}_{\max}(\rho^b)$ is more complicated in nonequilibrium cases. We know that the LGI function $\mathcal{I}_{\max}(t, \rho^b)$ is asymmetric in terms of temperature difference ΔT . We plot the MLGI function $\mathcal{I}_{\max}(\rho^b)$ with respect to detuning angle θ defined in (11) (with fixed λ) and nonequilibrium condition ΔT in FIG. 9. When the mean temperature is relatively low $T_m < \bar{\omega}$, detuning $\Delta\omega > 0$ or $\Delta\omega < 0$ can increase MLGI function $\mathcal{I}_{\max}(\rho^b)$

with $\Delta T < 0$ or $\Delta T > 0$ respectively, see FIG. 9 (a). In other words, the qubit with smaller frequency should couple with higher temperature bath and vice versa. Recall that in the low mean temperature regime, the MLGI function $\mathcal{I}_{\max}(\rho^b)$ is enhanced from increasing the nonlocal state population. One can check that the nonlocal state population sum is also increased by detuning $\Delta\omega > 0$ or $\Delta\omega < 0$ if $\Delta T < 0$ or $\Delta T > 0$. Intuitively we can understand that the low frequency qubit coupled with the high temperature bath can help the excitation, since the mean temperature is relatively low and the system is at the ground state with high probability. When the mean temperature is relatively large, i.e., $T_m \approx \bar{\omega}$, from FIG. 9 (b), we see that detuning $\Delta\omega$ will not enhance the violation of LGI significantly anymore for either $\Delta T > 0$ or $\Delta T < 0$. The asymmetric temperature contribution is obvious: $\Delta T > 0$ always gives stronger enhancement of MLGI function $\mathcal{I}_{\max}(\rho^b)$. In equilibrium environments, around $T_m \approx \bar{\omega}$, the MLGI function $\mathcal{I}_{\max}(\rho^{b,e})$ has the maximal value, see FIG. 2. Such maximal point is the result of the competition between the excitation of nonlocal states and the decoherence effect. In nonequilibrium case around $T_m \approx \bar{\omega}$, detuning the two qubits will not help the excitation. In fact, detuning the two qubits leads to the nonlocal state to be less entangled and therefore does not boost the LGI violation.

C. MLGI Enhanced by Nonequilibrium Fermionic Environments

When the two qubit system is coupled with the two Fermionic baths, we consider how the nonequilibrium condition given by $\Delta\mu = \mu_2 - \mu_1$ contributes to the violation of LGI. Same as Bosonic nonequilibrium setup, the coherent evolution \mathcal{M}_0 and dissipator \mathcal{M}_J do not commute with nonvanishing $\Delta\mu \neq 0$. However, we still can have closed form of Zassenhaus formula (59) in the first order of the coupling constant J . We have the first order LGI function $\mathcal{I}(t, \rho^f)$ with the nonequilibrium corrections:

$$\mathcal{I}^{(1)}(t, \rho^f) = 4tJ(\rho_{22}^f + \rho_{33}^f)(\cos(2\lambda t) - \cos(\lambda t)) + \frac{2J}{\lambda}(\Delta n_1 + \Delta n_2)(\rho_{11}^f - \rho_{44}^f)(\sin(2\lambda t) - 2\sin(\lambda t)) \quad (88)$$

with $\omega_1 = \omega_2$ and $\lambda \neq 0$. The nonequilibrium correction term is proportional to $(\Delta n_1 + \Delta n_2)$. We can approximate the first order MLGI function $\mathcal{I}_{\max}(\rho^f)$ by

$$\mathcal{I}_{\max}^{(1)}(\rho^f) \approx \mathcal{I}^{(1)}(t = \pi/(3\lambda), \rho^f), \quad (89)$$

which gives

$$\begin{aligned} \mathcal{I}_{\max}^{(0)}(\rho^f) + \mathcal{I}_{\max}^{(1)}(\rho^f) &= \left(\frac{1}{2} - \frac{4\pi J}{3\lambda}\right)(\rho_{22}^f + \rho_{33}^f) \\ &+ \frac{\sqrt{3}J}{\lambda}(\Delta n_1 + \Delta n_2)(\rho_{44}^f - \rho_{11}^f) \end{aligned} \quad (90)$$

The nonequilibrium term Δn_l (30c)-(30d) with $l = 1, 2$ is bounded $|\Delta n_l| < 1/2$ in Fermionic case. Nonequilibrium conditions $\Delta\mu > 0$ and $\Delta\mu < 0$ only have difference in $\mathcal{I}_{\max}^{(1)}(\rho^f)$ with magnitude in order J . In other words, the asymmetric nonequilibrium condition $\Delta\mu$ does not give significantly asymmetric MLGI function $\mathcal{I}_{\max}(\rho^f)$, unlike the Bosonic nonequilibrium case.

In equilibrium setup, we know that the resonant point $\bar{\mu} = \bar{\omega}$ gives the maximal MLGI. Analytically, with $\bar{\mu} = \bar{\omega}$, the population sum $\rho_{22}^f + \rho_{33}^f$ (up to first order coupling J) has

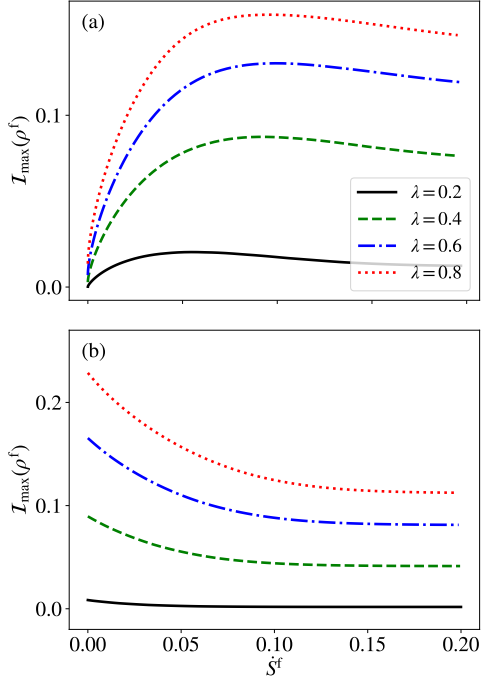


FIG. 10. The MLGI function $\mathcal{I}_{\max}(\rho^f)$ defined in (5) in term of the entropy production rate \dot{S}^f defined in (81) with the different inter-qubit coupling strength λ . (a) The chemical potential μ_1 is fixed with $\mu_1 = 0$ or (b) fixed with $\mu_1 = 1$. Other parameters are set as $\omega_1 = \omega_2 = 1$, $T_1 = T_2 = 0.2$ and $J = 0.05$.

the expression:

$$\rho_{22}^f + \rho_{33}^f = \frac{\cosh\left(\frac{\lambda}{2T}\right)}{\cosh\left(\frac{\Delta\mu}{2T}\right) + \cosh\left(\frac{\lambda}{2T}\right)} + \frac{\sinh^2\left(\frac{\Delta\mu}{2T}\right)}{2\left(\cosh\left(\frac{\Delta\mu+\lambda}{2T}\right) + 1\right)\left(\cosh\left(\frac{\Delta\mu-\lambda}{2T}\right) + 1\right)} \quad (91)$$

It is easy to see that the equilibrium setup $\Delta\mu = 0$ gives the maximal of population sum $\rho_{22}^f + \rho_{33}^f$. Therefore nonequilibrium condition does not give enhancement of MLGI $\mathcal{I}_{\max}(\rho^f)$ when $\bar{\mu} = \bar{\omega}$. See FIG. 7 for numerical results.

The major contribution up to the first order MLGI function in (90) is from $\rho_{22}^f + \rho_{33}^f$, which is the population sum of the non-local eigenstates. Away from the resonant point $\bar{\mu} = \bar{\omega}$, we can find that the population sum increases with the nonequilibrium condition $\Delta\mu$. Therefore, MLGI $\mathcal{I}_{\max}(\rho^f)$ can be enhanced by the nonequilibrium condition away from the resonant point. See FIG. 7 for numerical results that MLGI $\mathcal{I}_{\max}(\rho^f)$ can be enhanced by $\Delta\mu$ away from $\bar{\mu} = \bar{\omega}$.

The Fermionic environments with the different chemical potentials lead to the particle current flowing through the system. The nonequilibrium environments have the dissipation characterized by the entropy production rate \dot{S}^f defined in (78), see FIG. 6. The MLGI function $\mathcal{I}_{\max}(\rho^f)$ can be enhanced by consuming the nonequilibrium environments (with nonzero entropy production rate \dot{S}^f) if the chemical potentials

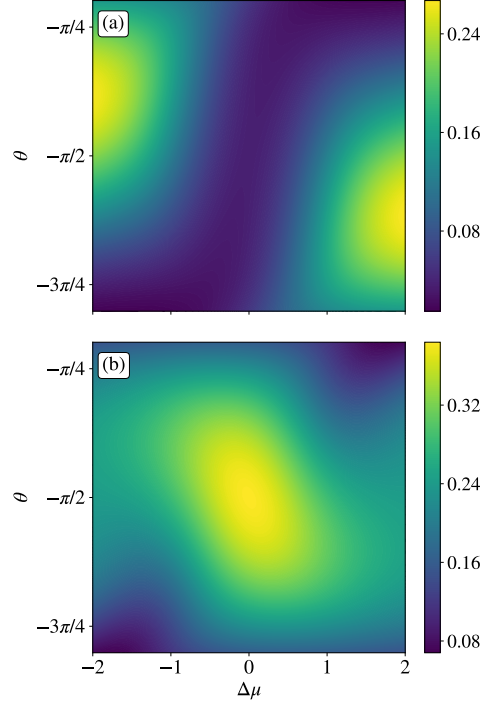


FIG. 11. The MLGI function $\mathcal{I}_{\max}(\rho^{ss})$ defined in (5) in terms of nonequilibrium condition $\Delta\mu = \mu_2 - \mu_1$ (nonequilibrium Fermionic bath with $T = 0.2$) and detuning angle θ defined in (11) with fixed $\lambda = 1$. (a) Small mean chemical potential $\mu_m = 0.2$ and (b) large mean chemical potential $\mu_m = 0.8$. Other parameters are set as $\bar{\omega}_1 = 1$ and $J = 0.005$.

μ_1 and μ_2 are away from the resonant point $\bar{\omega}$. For example, if we fix the chemical potential μ_1 at $\mu_1 = 0$, increasing the entropy production rate \dot{S}^f gives the enhancement of LGI violation, see FIG. 10. However, if we fix the μ_1 around the value $\bar{\omega}$, the nonequilibrium thermodynamic cost gives the smaller or zero MLGI function $\mathcal{I}_{\max}(\rho^f)$, see FIG. 10. The equilibrium case $\mu_1 = \mu_2 \approx \bar{\omega}$ with zero entropy production rate \dot{S}^f already gives almost saturated populations $\rho_{22}^f + \rho_{33}^f$, therefore the nonequilibrium cost \dot{S}^f does not enhance the LGI violation. Similarly with Bosonic environments, stronger inter-qubit coupling λ always increase the LGI violation either μ_1 and μ_2 away from or around the value $\bar{\omega}$.

We also studied how the detuning frequency $\Delta\omega$ combined with nonequilibrium condition $\Delta\mu$ contributes to the violation of LGI. Numerically, we separately contour plot the two-dimensional diagram of the MLGI $\mathcal{I}_{\max}(\rho^f)$ in terms of the nonequilibrium condition $\Delta\mu$ and the detuning angle θ (defined in (11)) with fixed tunneling strength λ , when the system is away from the resonant point or around the resonant point $\bar{\mu} = \bar{\omega}$, see FIG. (11). When the system is away $\bar{\mu} = \bar{\omega}$, lower frequency qubit should couple the higher chemical potential reservoir and higher frequency qubit should couple the lower chemical potential reservoir, in order to reach the larger violation of LGI. However, around resonant point, detuning the system $\omega_1 \neq \omega_2$ with nonequilibrium condition $\Delta\mu$ does not give larger violation of LGI. The explanations are still based

on the population sum $\rho_{22}^f + \rho_{33}^f$ in terms of the detuning angle θ and the nonequilibrium condition $\Delta\mu$. Away from the resonant point, the system (with high probability) stays at ground states or highest excited states which has classical description. Then detuning the two qubits by $\Delta\omega$ or by nonequilibrium condition $\Delta\mu > 0$ (or $\Delta\mu < 0$), we can increase the nonlocal state (the first and the second excited states) population. On the contrary, around resonant point, the nonequilibrium condition always gives less population of nonlocal states.

VI. CONCLUSION

We have studied LGI violation in quantum system (two interacting qubits) coupled with equilibrium or nonequilibrium environments. Each qubit is coupled with one (Bosonic or Fermionic) bath. We have derived evolution equation of the reduced density matrix beyond secular approximation (Bloch-Redfield equation). There are analytical solutions of the reduced density matrix of steady states. We calculate the heat current (the system coupled with the nonequilibrium Bosonic environments) or the particle current (the system coupled with the nonequilibrium Fermionic environments) in the steady state regime. Correspondingly, we study the entropy production rate as the nonequilibrium thermodynamic cost. We use the maximal value to LGI function $\mathcal{I}(t, \rho^{ss})$, which is called MLGI function $\mathcal{I}_{\max}(\rho^{ss})$ defined in (5), to quantify the degree of LGI violation. We have obtained the analytical form of both LGI function $\mathcal{I}(t, \rho^{ss})$ and MLGI function $\mathcal{I}_{\max}(\rho^{ss})$ in the zeroth order and the first order of coupling J . The zeroth order represents the coherent evolution and the first order describes the non-unitary part (due to coupled with the environments). We also analytically separate the equilibrium and nonequilibrium effects in the first order LGI function $\mathcal{I}(t, \rho^{ss})$ and MLGI function $\mathcal{I}_{\max}(\rho^{ss})$.

In equilibrium set up, LGI violation is caused by unitary evolution of the first and the second excited states (entangled states in two qubit system). In Bosonic case, MLGI function $\mathcal{I}_{\max}(\rho^{b,e})$ has non-monotonic relationship with the equilibrium temperature. The analytical results reveal that the environment can give excitations and therefore the nonlocal eigenstates (enhance LGI violation) but can also have decoherence effect (reduce LGI violation). Fermionic bath has similar results.

The nonequilibrium condition can be quantified by the temperature difference or chemical potential difference for Bosonic or Fermionic reservoir respectively. The entropy production rate also characterizes the thermodynamic nonequilibrium cost. In Bosonic case, nonequilibrium environment can magnify the violation of LGI function (increasing the MLGI function $\mathcal{I}_{\max}(\rho^b)$ by temperature difference), if the mean temperature is relatively low. Correspondingly, the LGI violation enhancement monotonically increases with the entropy production rate. In particular, MLGI function $\mathcal{I}_{\max}(\rho^b)$ can be enhanced more if $T_2 > T_1$ (we measure the local observable in qubit 1). Such asymmetric result is beyond Lindbald description (wiped out by secular approximation). In Fermionic bath, we have the MLGI function $\mathcal{I}_{\max}(\rho^b)$ enhancement by

the nonequilibrium condition $\Delta\mu$ (chemical potential difference) if the system is away from the resonant point $\bar{\mu} = \bar{\omega}$. Such enhancement is realized by the thermodynamic nonequilibrium cost (nonzero entropy production rate). When we have detuned two qubits (different frequencies), the low (high) frequency qubit should couple to high (low) temperature or chemical potential (with low temperature) bath in order to enhance LGI violation.

Whether we can realize the macroscopic coherence or Shrödinger's cat in the experiments is a very important fundamental question in quantum mechanics. The inevitable coupling with environments leads to the decoherence (classical macroscopic realism description). Our study suggests new ways to test the macroscopic realism via the LGI. We can take the advantage from coupling with the environments by designing nonlocal excited states of the system. Furthermore, with the detuning of the two-qubit system, the nonequilibrium environments (with different temperatures or chemical potentials) can significantly enhance the degree of the violation of LGI. In our model, we describe quite general environments. Our results are not based on the sophisticated designed interaction between the system and the environments. It is much easier to create a system coupled with the nonequilibrium environments than a completely decoupled system. It is expected that our results can be generalized into multi-qubit system coupled with multi-nonequilibrium environments.

ACKNOWLEDGMENTS

K.Z. and J.W. thank the supports from Grant No. NSF-PHY 76066 and NSF-CHE-1808474. W.W. is supported by the National Natural Science Foundation of China under Grant No. 11905222. We thank Prof. Jason Kestner, Prof. Vladimir Korepin, and Xuanhua Wang for helpful discussions.

Appendix A: Transition Matrix Elements for Time Evolution Equation

Matrix \mathcal{M} defined in (23) describing the time evolution of the system based on Bloch-Redfield equation (17) has the matrix elements $\mathcal{M}_{ab,cd}$ (with row index ab and column index cd):

$$\mathcal{M}_{11,11} = -2 \left(\cos^2 \frac{\theta}{2} (\alpha_1(\omega'_1) + \alpha_2(\omega'_2)) + \sin^2 \frac{\theta}{2} (\alpha_1(\omega'_2) + \alpha_2(\omega'_1)) \right); \quad (A1)$$

$$\mathcal{M}_{11,22} = \mathcal{M}_{33,44} = 2 \left(\cos^2 \frac{\theta}{2} \beta_1(\omega'_1) + \sin^2 \frac{\theta}{2} \beta_2(\omega'_1) \right); \quad (A2)$$

$$\mathcal{M}_{11,33} = \mathcal{M}_{22,44} = 2 \left(\sin^2 \frac{\theta}{2} \beta_1(\omega'_2) + \cos^2 \frac{\theta}{2} \beta_2(\omega'_2) \right); \quad (A3)$$

$$\mathcal{M}_{22,11} = \mathcal{M}_{44,33} = 2 \left(\cos^2 \frac{\theta}{2} \alpha_1(\omega'_1) + \sin^2 \frac{\theta}{2} \alpha_2(\omega'_1) \right); \quad (\text{A4})$$

$$\begin{aligned} \mathcal{M}_{22,22} = -2 \left(\cos^2 \frac{\theta}{2} (\beta_1(\omega'_1) + \alpha_2(\omega'_2)) \right. \\ \left. + \sin^2 \frac{\theta}{2} (\alpha_1(\omega'_2) + \beta_2(\omega'_1)) \right); \end{aligned} \quad (\text{A5})$$

$$\mathcal{M}_{33,11} = \mathcal{M}_{44,22} = 2 \left(\sin^2 \frac{\theta}{2} \alpha_1(\omega'_2) + \cos^2 \frac{\theta}{2} \alpha_2(\omega'_2) \right); \quad (\text{A6})$$

$$\begin{aligned} \mathcal{M}_{33,33} = -2 \left(\cos^2 \frac{\theta}{2} (\alpha_1(\omega'_1) + \beta_2(\omega'_2)) \right. \\ \left. + \sin^2 \frac{\theta}{2} (\alpha_2(\omega'_1) + \beta_1(\omega'_2)) \right); \end{aligned} \quad (\text{A7})$$

$$\begin{aligned} \mathcal{M}_{44,44} = -2 \left(\cos^2 \frac{\theta}{2} (\beta_1(\omega'_1) + \beta_2(\omega'_2)) \right. \\ \left. + \sin^2 \frac{\theta}{2} (\beta_1(\omega'_2) + \beta_2(\omega'_1)) \right); \end{aligned} \quad (\text{A8})$$

$$\begin{aligned} \mathcal{M}_{11,23} = \mathcal{M}_{11,32} = -\mathcal{M}_{23,44} = -\mathcal{M}_{32,44} \\ = \frac{1}{2} \sin \theta (\beta_2(\omega'_1) + \beta_2(\omega'_2) - \beta_1(\omega'_1) - \beta_1(\omega'_2)); \end{aligned} \quad (\text{A9})$$

$$\begin{aligned} \mathcal{M}_{22,23} = \mathcal{M}_{22,32} = \mathcal{M}_{23,33} = \mathcal{M}_{32,33} \\ = \frac{1}{2} \sin \theta (\alpha_2(\omega'_1) + \beta_1(\omega'_2) - \alpha_1(\omega'_1) - \beta_2(\omega'_2)); \end{aligned} \quad (\text{A10})$$

$$\begin{aligned} \mathcal{M}_{33,23} = \mathcal{M}_{33,32} = \mathcal{M}_{23,22} = \mathcal{M}_{32,22} \\ = \frac{1}{2} \sin \theta (\beta_1(\omega'_1) + \alpha_2(\omega'_2) - \alpha_1(\omega'_2) - \beta_2(\omega'_1)); \end{aligned} \quad (\text{A11})$$

$$\begin{aligned} \mathcal{M}_{44,23} = \mathcal{M}_{44,32} = -\mathcal{M}_{23,11} = -\mathcal{M}_{32,11} \\ = \frac{1}{2} \sin \theta (\alpha_1(\omega'_1) + \alpha_1(\omega'_2) - \alpha_2(\omega'_1) - \alpha_2(\omega'_2)); \end{aligned} \quad (\text{A12})$$

$$\begin{aligned} \mathcal{M}_{23,23} = \mathcal{M}_{23,23}^* = i\Omega \\ - \left(\cos^2 \frac{\theta}{2} (\alpha_1(\omega'_1) + \alpha_2(\omega'_2) + \beta_1(\omega'_1) + \beta_2(\omega'_2)) \right. \\ \left. + \sin^2 \frac{\theta}{2} (\alpha_2(\omega'_1) + \alpha_1(\omega'_2) + \beta_2(\omega'_1) + \beta_1(\omega'_2)) \right) \end{aligned} \quad (\text{A13})$$

$$\begin{aligned} \mathcal{M}_{11,44} = \mathcal{M}_{44,11} = \mathcal{M}_{22,33} \\ = \mathcal{M}_{33,22} = \mathcal{M}_{23,32} = \mathcal{M}_{32,23} = 0 \end{aligned} \quad (\text{A14})$$

Parameters $\alpha_l(\omega)$ and $\beta_l(\omega)$ with $l = 1, 2$ are defined in (19). Angle θ defined in (11) tells the detuning frequency $\Delta\omega$ of the two qubits.

Appendix B: Elements of Steady State Population Matrix

Steady state population matrix defined in (27) has the matrix elements when the two baths are Bosonic or Fermionic

(with symmetric constant coupling $J_1(\omega) = J_2(\omega) = J$)

$$\mathcal{A}_{aa,bb} = \mathcal{M}_{aa,bb} + \frac{\kappa^{\text{bf}}}{J} \mathcal{M}_{aa,23} \mathcal{M}_{23,bb} \quad (\text{B1})$$

with coefficient κ^{b} for Bosonic bath defined in (33) and coefficient κ^{f} for Fermionic bath defined in (43).

1. Elements of Steady State Population Matrix for Bosonic Bath

The explicit expressions for the matrix elements \mathcal{A} , when the two baths are Bosonic, are:

$$\mathcal{A}_{11,11}^{\text{b}} = -2(\tilde{n}_1 + \tilde{n}_2) + \kappa_b (\Delta n_1 + \Delta n_2)^2 \quad (\text{B2})$$

$$\mathcal{A}_{11,22}^{\text{b}} = 2(\tilde{n}_1 + 1) + \kappa_b (\Delta n_2^2 - \Delta n_1^2) \quad (\text{B3})$$

$$\mathcal{A}_{11,33}^{\text{b}} = 2(\tilde{n}_2 + 1) + \kappa_b (\Delta n_1^2 - \Delta n_2^2) \quad (\text{B4})$$

$$\mathcal{A}_{11,44}^{\text{b}} = -\kappa_b (\Delta n_1 + \Delta n_2)^2 \quad (\text{B5})$$

$$\mathcal{A}_{22,11}^{\text{b}} = 2\tilde{n}_1 + \kappa_b (\Delta n_1^2 - \Delta n_2^2) \quad (\text{B6})$$

$$\mathcal{A}_{22,22}^{\text{b}} = -2(\tilde{n}_1 + \tilde{n}_2 + 1) - \kappa_b (\Delta n_1 - \Delta n_2)^2 \quad (\text{B7})$$

$$\mathcal{A}_{22,33}^{\text{b}} = \kappa_b (\Delta n_1 - \Delta n_2)^2 \quad (\text{B8})$$

$$\mathcal{A}_{22,44}^{\text{b}} = 2(\tilde{n}_2 + 1) - \kappa_b (\Delta n_1^2 - \Delta n_2^2) \quad (\text{B9})$$

$$\mathcal{A}_{33,11}^{\text{b}} = 2\tilde{n}_2 - \kappa_b (\Delta n_1^2 - \Delta n_2^2) \quad (\text{B10})$$

$$\mathcal{A}_{33,22}^{\text{b}} = \kappa_b (\Delta n_2 - \Delta n_1)^2 \quad (\text{B11})$$

$$\mathcal{A}_{33,33}^{\text{b}} = -2(\tilde{n}_1 + \tilde{n}_2 + 1) - \kappa_b (\Delta n_1 - \Delta n_2)^2 \quad (\text{B12})$$

$$\mathcal{A}_{33,44}^{\text{b}} = 2(\tilde{n}_1 + 1) + \kappa_b (\Delta n_1^2 - \Delta n_2^2) \quad (\text{B13})$$

$$\mathcal{A}_{44,11}^{\text{b}} = -\kappa_b (\Delta n_1 + \Delta n_2)^2 \quad (\text{B14})$$

$$\mathcal{A}_{44,22}^{\text{b}} = 2\tilde{n}_2 + \kappa_b (\Delta n_1^2 - \Delta n_2^2) \quad (\text{B15})$$

$$\mathcal{A}_{44,33}^{\text{b}} = 2\tilde{n}_1 - \kappa_b (\Delta n_1^2 - \Delta n_2^2) \quad (\text{B16})$$

$$\mathcal{A}_{44,44}^{\text{b}} = -2(\tilde{n}_1 + \tilde{n}_2 + 2) + \kappa_b (\Delta n_1 + \Delta n_2)^2 \quad (\text{B17})$$

Notations \tilde{n}_l and Δ with $l = 1, 2$ are defined in (30a)-(30c). Note that the overall constant J in matrix \mathcal{A} has omitted here.

2. Matrix Elements of Steady State Population Matrix for Fermionic Bath

The explicit expressions for the matrix elements \mathcal{A} , when the two bath are Fermionic, are:

$$\mathcal{A}_{11,11}^{\text{f}} = -2(\tilde{n}_1 + \tilde{n}_2) + \kappa_f (\Delta n_1 + \Delta n_2)^2 \quad (\text{B18})$$

$$\mathcal{A}_{11,22}^{\text{f}} = 2(1 - \tilde{n}_1) - \kappa_f (\Delta n_1 + \Delta n_2)^2 \quad (\text{B19})$$

$$\mathcal{A}_{11,33}^{\text{f}} = 2(1 - \tilde{n}_2) - \kappa_f (\Delta n_1 + \Delta n_2)^2 \quad (\text{B20})$$

$$\mathcal{A}_{11,44}^{\text{f}} = -\kappa_f (\Delta n_1 + \Delta n_2)^2 \quad (\text{B21})$$

$$\mathcal{A}_{22,11}^{\text{f}} = 2\tilde{n}_1 + \kappa_f (\Delta n_1 + \Delta n_2)^2 \quad (\text{B22})$$

$$\mathcal{A}_{22,22}^{\text{f}} = 2(\tilde{n}_1 - \tilde{n}_2 - 1) + \kappa_f (\Delta n_1 + \Delta n_2)^2 \quad (\text{B23})$$

$$\mathcal{A}_{22,44}^f = 2(1 - \tilde{n}_2) + \kappa_f (\Delta n_1 + \Delta n_2)^2 \quad (B24)$$

$$\mathcal{A}_{33,11}^f = 2\tilde{n}_2 + \kappa_f (\Delta n_1 + \Delta n_2)^2 \quad (B25)$$

$$\mathcal{A}_{33,22}^f = \kappa_f (\Delta n_1 + \Delta n_2)^2 \quad (B26)$$

$$\mathcal{A}_{33,33}^f = 2(\tilde{n}_2 - \tilde{n}_1 - 1) + \kappa_f (\Delta n_1 + \Delta n_2)^2 \quad (B27)$$

$$\mathcal{A}_{44,11}^f = -\kappa_f (\Delta n_1 + \Delta n_2)^2 \quad (B28)$$

$$\mathcal{A}_{44,22}^f = 2\tilde{n}_2 - \kappa_f (\Delta n_1 + \Delta n_2)^2 \quad (B29)$$

$$\mathcal{A}_{44,33}^f = 2\tilde{n}_1 - \kappa_f (\Delta n_1 + \Delta n_2)^2 \quad (B30)$$

$$\mathcal{A}_{44,44}^f = 2(\tilde{n}_1 + \tilde{n}_2 - 2) - \kappa_f (\Delta n_1 + \Delta n_2)^2 \quad (B31)$$

Notations \tilde{n}_l and Δ with $l = 1, 2$ are defined in (30a)-(30c).

Appendix C: Steady State Heat/Particle Current

Given the steady state of nonequilibrium Bosonic baths in (32a)-(32d), the heat current I_2^b defined in (74) has the form

$$\begin{aligned} I_2^b = & -2(\cos^2 \frac{\theta}{2} \alpha_1(\omega'_1) \omega'_1 + \sin^2 \frac{\theta}{2} \alpha_1(\omega'_2) \omega'_2) \rho_{11}^b \\ & + 2(\cos^2 \frac{\theta}{2} \beta_1(\omega'_1) \omega'_1 - \sin^2 \frac{\theta}{2} \alpha_1(\omega'_2) \omega'_2) \rho_{22}^b \\ & + 2(\sin^2 \frac{\theta}{2} \beta_1(\omega'_2) \omega'_2 - \cos^2 \frac{\theta}{2} \alpha_1(\omega'_1) \omega'_1) \rho_{33}^b \end{aligned}$$

$$\begin{aligned} & + 2(\cos^2 \frac{\theta}{2} \beta_1(\omega'_1) \omega'_1 + \sin^2 \frac{\theta}{2} \beta_1(\omega'_2) \omega'_2) \rho_{44}^b \\ & - \frac{1}{2} \sin \theta (\beta_1(\omega'_2) + \alpha_1(\omega'_2)) \omega'_1 (\rho_{23}^b + \rho_{32}^b) \\ & - \frac{1}{2} \sin \theta (\beta_1(\omega'_1) + \alpha_1(\omega'_1)) \omega'_2 (\rho_{23}^b + \rho_{32}^b) \end{aligned} \quad (C1)$$

where the parameters $\alpha_1(\omega)$ and $\beta_1(\omega)$ are defined in (19). Note that the occupation particle number obeys the Boson-Einstein distribution.

Given the steady state of nonequilibrium Fermionic baths in (42a)-(42d), the particle current I_2^f defined in (78) has the form

$$\begin{aligned} I_2^f = & -2(\cos^2 \frac{\theta}{2} \alpha_1(\omega'_1) + \sin^2 \frac{\theta}{2} \alpha_1(\omega'_2)) \rho_{11}^f \\ & + 2(\cos^2 \frac{\theta}{2} \beta_1(\omega'_1) - \sin^2 \frac{\theta}{2} \alpha_1(\omega'_2)) \rho_{22}^f \\ & + 2(\sin^2 \frac{\theta}{2} \beta_1(\omega'_2) - \cos^2 \frac{\theta}{2} \alpha_1(\omega'_1)) \rho_{33}^f \\ & + 2(\cos^2 \frac{\theta}{2} \beta_1(\omega'_1) + \sin^2 \frac{\theta}{2} \beta_1(\omega'_2)) \rho_{44}^f \\ & - \frac{1}{2} \sin \theta (\beta_1(\omega'_2) + \alpha_1(\omega'_2)) (\rho_{23}^f + \rho_{32}^f) \\ & - \frac{1}{2} \sin \theta (\beta_1(\omega'_1) + \alpha_1(\omega'_1)) (\rho_{23}^f + \rho_{32}^f) \end{aligned} \quad (C2)$$

where the parameters $\alpha_1(\omega)$ and $\beta_1(\omega)$ are defined in (19). Note that the occupation particle number obeys the Fermi-Dirac distribution.

[1] M. A. Nielsen and I. L. Chuang, Quantum computation and quantum information (2010).

[2] R. Horodecki, P. Horodecki, M. Horodecki, and K. Horodecki, *Reviews of Modern Physics* **81**, 865 (2009).

[3] K. Modi, A. Brodutch, H. Cable, T. Paterek, and V. Vedral, *Reviews of Modern Physics* **84**, 1655 (2012).

[4] J. S. Bell, *Physics Physique Fizika* **1**, 195 (1964).

[5] S. J. Freedman and J. F. Clauser, *Physical Review Letters* **28**, 938 (1972).

[6] B. Hensen, H. Bernien, A. E. Dréau, A. Reiserer, N. Kalb, M. S. Blok, J. Ruitenberg, R. F. Vermeulen, R. N. Schouten, C. Abellán, *et al.*, *Nature* **526**, 682 (2015).

[7] N. Brunner, D. Cavalcanti, S. Pironio, V. Scarani, and S. Wehner, *Reviews of Modern Physics* **86**, 419 (2014).

[8] A. J. Leggett and A. Garg, *Physical Review Letters* **54**, 857 (1985).

[9] C. Emery, N. Lambert, and F. Nori, *Reports on Progress in Physics* **77**, 016001 (2013).

[10] M. Markiewicz, P. Kurzyński, J. Thompson, S.-Y. Lee, A. Soeda, T. Paterek, and D. Kaszlikowski, *Physical Review A* **89**, 042109 (2014).

[11] L. Clemente and J. Kofler, *Physical review letters* **116**, 150401 (2016).

[12] D. Saha, S. Mal, P. K. Panigrahi, and D. Home, *Physical Review A* **91**, 032117 (2015).

[13] J. Kofler and Č. Brukner, *Physical Review A* **87**, 052115 (2013).

[14] C. H. Van Der Wal, A. Ter Haar, F. Wilhelm, R. Schouten, C. Harmans, T. Orlando, S. Lloyd, and J. Mooij, *Science* **290**, 773 (2000).

[15] A. Palacios-Laloy, F. Mallet, F. Nguyen, P. Bertet, D. Vion, D. Esteve, and A. N. Korotkov, *Nature Physics* **6**, 442 (2010).

[16] M. Goggin, M. Almeida, M. Barbieri, B. Lanyon, J. Obrien, A. White, and G. Pryde, *Proceedings of the National Academy of Sciences* **108**, 1256 (2011).

[17] V. Athalye, S. S. Roy, and T. Mahesh, *Physical Review Letters* **107**, 130402 (2011).

[18] G. C. Knee, S. Simmons, E. M. Gauger, J. J. Morton, H. Riemann, N. V. Abrosimov, P. Becker, H.-J. Pohl, K. M. Itoh, M. L. Thewalt, *et al.*, *Nature Communications* **3**, 606 (2012).

[19] Z.-Q. Zhou, S. F. Huelga, C.-F. Li, and G.-C. Guo, *Physical Review Letters* **115**, 113002 (2015).

[20] J. Formaggio, D. Kaiser, M. Murskyj, and T. Weiss, *Physical review letters* **117**, 050402 (2016).

[21] A. J. Leggett, S. Chakravarty, A. T. Dorsey, M. P. Fisher, A. Garg, and W. Zwerger, *Reviews of Modern Physics* **59**, 1 (1987).

[22] H.-P. Breuer and F. Petruccione, *The theory of open quantum systems* (Oxford University Press on Demand, 2002).

[23] W. H. Zurek, *Reviews of Modern Physics* **75**, 715 (2003).

[24] M. O. Scully and M. S. Zubairy, *Quantum optics* (1999).

[25] I. De Vega and D. Alonso, *Reviews of Modern Physics* **89**, 015001 (2017).

[26] C. Emery, *Physical Review A* **87**, 032106 (2013).

[27] G.-Y. Chen, S.-L. Chen, C.-M. Li, and Y.-N. Chen, *Scientific*

Reports **3**, 2514 (2013).

[28] M. Łobejko, J. Łuczka, and J. Dajka, Physical Review A **91**, 042113 (2015).

[29] A. Friedenberger and E. Lutz, Physical Review A **95**, 022101 (2017).

[30] T. Chanda, T. Das, S. Mal, A. Sen, U. Sen, *et al.*, Physical Review A **98**, 022138 (2018).

[31] J. C. Castillo, F. J. Rodríguez, and L. Quiroga, Physical Review A **88**, 022104 (2013).

[32] P.-W. Chen and M. M. Ali, Scientific Reports **4**, 6165 (2014).

[33] S. Datta, S. Mal, and A. S. Majumdar, arXiv preprint arXiv:1808.10345 (2018).

[34] N. Lambert, C. Emery, Y.-N. Chen, and F. Nori, Physical Review Letters **105**, 176801 (2010).

[35] C. Addis, G. Brebner, P. Haikka, and S. Maniscalco, Physical Review A **89**, 024101 (2014).

[36] Y.-J. Zhang, W. Han, Y.-J. Xia, Y.-M. Yu, and H. Fan, Scientific Reports **5**, 13359 (2015).

[37] G. Guarneri, M. Kolář, and R. Filip, Physical Review Letters **121**, 070401 (2018).

[38] M. B. Plenio, S. Huelga, A. Beige, and P. Knight, Physical Review A **59**, 2468 (1999).

[39] M. Arnesen, S. Bose, and V. Vedral, Physical Review Letters **87**, 017901 (2001).

[40] X. Wang, Physical Review A **64**, 012313 (2001).

[41] G. L. Kamta and A. F. Starace, Physical Review Letters **88**, 107901 (2002).

[42] D. Braun, Physical Review Letters **89**, 277901 (2002).

[43] F. Benatti, R. Floreanini, and M. Piani, Physical Review Letters **91**, 070402 (2003).

[44] F. Verstraete, M. M. Wolf, and J. I. Cirac, Nature Physics **5**, 633 (2009).

[45] X. Zhao, J. Jing, B. Corn, and T. Yu, Physical Review A **84**, 032101 (2011).

[46] S. F. Huelga, A. Rivas, and M. B. Plenio, Physical review letters **108**, 160402 (2012).

[47] M. Esposito, U. Harbola, and S. Mukamel, Reviews of Modern Physics **81**, 1665 (2009).

[48] Z. Zhang and J. Wang, The Journal of chemical physics **140**, 06B622_1 (2014).

[49] S.-W. Li, C. Cai, and C. Sun, Annals of Physics **360**, 19 (2015).

[50] Z. Wang, W. Wu, G. Cui, and J. Wang, New Journal of Physics **20**, 033034 (2018).

[51] N. Lambert, R. Aguado, and T. Brandes, Physical Review B **75**, 045340 (2007).

[52] L. Quiroga, F. J. Rodriguez, M. E. Ramirez, and R. Paris, Physical Review A **75**, 032308 (2007).

[53] I. Sinaysky, F. Petruccione, and D. Burgarth, Physical Review A **78**, 062301 (2008).

[54] L.-A. Wu and D. Segal, Physical Review A **84**, 012319 (2011).

[55] J.-Q. Liao, J.-F. Huang, L.-M. Kuang, *et al.*, Physical Review A **83**, 052110 (2011).

[56] A. Dhar, K. Saito, and P. Hänggi, Physical Review E **85**, 011126 (2012).

[57] B. Bellomo and M. Antezza, EPL (Europhysics Letters) **104**, 10006 (2013).

[58] Z. Zhang and J. Wang, New Journal of Physics **17**, 043053 (2015).

[59] Z. Wang, W. Wu, and J. Wang, Physical Review A **99**, 042320 (2019).

[60] A. Tavakoli, G. Haack, M. Huber, N. Brunner, and J. B. Brask, Quantum **2**, 73 (2018).

[61] F. Tacchino, A. Auffèves, M. Santos, and D. Gerace, Physical Review Letters **120**, 063604 (2018).

[62] X. Wang and J. Wang, Physical Review A **100**, 052331 (2019).

[63] J. Mendoza-Arenas, F. Gómez-Ruiz, F. Rodríguez, and L. Quiroga, Scientific Reports **9**, 1 (2019).

[64] F. Bloch, Physical Review **105**, 1206 (1957).

[65] A. G. Redfield, IBM Journal of Research and Development **1**, 19 (1957).

[66] A. Suárez, R. Silbey, and I. Oppenheim, The Journal of Chemical Physics **97**, 5101 (1992).

[67] J. Jeske, D. J. Ing, M. B. Plenio, S. F. Huelga, and J. H. Cole, The Journal of Chemical Physics **142**, 064104 (2015).

[68] D. Farina and V. Giovannetti, arXiv preprint arXiv:1903.07324 (2019).

[69] D. Petrosyan and G. Kurizki, Physical Review Letters **89**, 207902 (2002).

[70] E. Lieb, T. Schultz, and D. Mattis, Annals of Physics **16**, 407 (1961).

[71] S. Sachdev, Handbook of Magnetism and Advanced Magnetic Materials (2007).

[72] T. Kimura, Progress of Theoretical and Experimental Physics **2017** (2017).